

Article

Digital Twin Enabled Process Development, Optimization and Control in Lyophilization for Enhanced Biopharmaceutical Production

Alex Juckers ^{1,2} , Petra Knerr ², Frank Harms ² and Jochen Strube ^{1,*}

¹ Institute for Separation and Process Technology, Clausthal University of Technology, 38678 Clausthal-Zellerfeld, Germany

² Martin Christ Gefriertrocknungsanlagen GmbH, 37520 Osterode am Harz, Germany

* Correspondence: strube@itv.tu-clausthal.de

Abstract: Digital twins have emerged as a powerful concept for real-time monitoring and analysis, facilitating Quality by Design integration into biopharmaceutical manufacturing. Traditionally, lyophilization processes are developed through trial-and-error, incorporating high security margins and inflexible process set points. Digital twins enable the integration of adaptable operating conditions and implementation of automation through Advanced Process Control (APC) with Process Analytical Technology (PAT) and validated physicochemical models that rely on heat and mass transfer principles, allowing us to overcome the challenges imposed by the lyophilization process. In this study, a digital twin for freeze-drying processes is developed and experimentally validated. Using the digital twin, primary drying conditions were optimized for controlled nucleation and annealing methods by carrying out a few laboratory tests beforehand. By incorporating PAT and modeling, the digital twin accurately predicts the product's temperature and drying endpoint, showing smaller errors than the experiments. The digital twin significantly increases productivity by up to 300% while reducing the costs by 74% and the Global Warming Potential by 64%.

Keywords: lyophilization; Process Analytical Technology; process modeling; Quality by Design; digital twin; process optimization; Advanced Process Control; controlled nucleation



Citation: Juckers, A.; Knerr, P.; Harms, F.; Strube, J. Digital Twin Enabled Process Development, Optimization and Control in Lyophilization for Enhanced Biopharmaceutical Production. *Processes* **2024**, *12*, 211. <https://doi.org/10.3390/pr12010211>

Academic Editors: Roberto Pisano and Raul D. S. G. Campilho

Received: 10 August 2023

Revised: 13 November 2023

Accepted: 4 January 2024

Published: 18 January 2024



Copyright: © 2024 by the authors. Licensee MDPI, Basel, Switzerland. This article is an open access article distributed under the terms and conditions of the Creative Commons Attribution (CC BY) license (<https://creativecommons.org/licenses/by/4.0/>).

1. Introduction

Freeze-drying, also known as lyophilization, plays a critical role in the pharmaceutical industry for the production of high-quality medications [1]. Approximately 16% of the TOP100 medications are freeze-dried [2]. The process consists of three distinct phases: freezing, primary and secondary drying. During the freezing phase, the liquid water is transformed into solid ice. In the subsequent primary drying, the solid ice is removed via sublimation, and in the following secondary drying, the remaining bound water is removed via desorption to achieve the desired residual moisture.

Lyophilization offers several challenges to process design:

- Nucleation [3–5]: in typical lyophilization processes, the degree of supercooling and the nucleation time are not controlled, resulting in intra- and inter-batch variability in ice crystal size and distribution, and, hence, a variable pore structure in the final freeze-dried product.
- Edge effects [6,7]: during primary drying, vials that are positioned on the outside of the shelf receive more heat than center vials due to radiation and nesting effects, resulting in higher product temperatures in edge vials.
- Process dynamics [8]: the product temperature is a function of shelf temperature and chamber pressure and cannot be directly controlled.

Typically, lyophilization processes are developed using a trial-and-error approach that relies heavily on empirical values, causing high experimental workloads. The resulting

process is then validated and remains unchanged throughout the entire product's life cycle, incorporating significant safety margins [9,10]. Here, a paradigm shift away from Quality by Testing towards Quality by Design (QbD) is necessary to design robust and efficient processes [11–13]. QbD is a systemic, science-based method that focuses on process understanding and enables continuous data-driven process improvement [14].

Process Analytical Technology (PAT) plays a crucial role in QbD implementation. It enables in-process data collection, real-time analysis and decision making. By integrating PAT, deep process understanding, control and reduced quality variability can be achieved. For lyophilization, several PAT tools are available: controlled nucleation [3,5,15–18], temperature sensors (wired or wireless), comparative pressure measurement [19–25], near-infrared and Raman spectroscopy [26–37], heat flux sensors [38–43], mass spectrometry [24,44–46], manometric temperature measurement (MTM) [9,19,20,22,24,45,47–52], and tunable diode laser absorption spectroscopy [53–59].

Besides PAT, modeling plays an important role in QbD implementation. It provides an irreplaceable tool for predicting and optimizing process parameters, facilitating the design of robust processes to achieve the desired product attributes. By simulating different process conditions, potential risks can be identified and addressed prior to actual implementation. Modeling can help optimize process parameters, reduce the experimental workload, and eliminate the need for costly and time-consuming trial-and-error approaches. Fully dynamic models (sorption–sublimation) use complex mathematical descriptions to explain the process dynamics that require time-consuming solution approaches [8,60–69]. To reduce the complexity of these models, a simplified model has been developed that assumes pseudo-stationary conditions during primary drying [20,70–84], leading to faster solutions while reducing the resolution of the effects [70]. Process optimization has been achieved through the utilization of these process models [61,74–76,78–80,84].

By utilizing real-time data from PAT and incorporating these into a dynamic model, it is possible to create a digital twin that reflects the current state and behavior of the system. The difference between elementary digital models and comprehensive digital twins is determined by the modeling complexity and the degree of information exchange with the physical system (see Figure 1) [85]. Digital twins lay the foundation for the implementation of manufacturing processes that operate under proven acceptable ranges (PAR) rather than fixed set points, revealing the optimization potential of conventional processes [86–88].

In this work, a digital twin for the lyophilization process is developed, combining the previous scientific work of the authors [18–20,89], and validated against experiments. Figure 2 shows the digital twin concept. Comparative pressure measurement is used for endpoint detection and as a forwarding condition to secondary drying. MTM enables online model parameter determination of the dry layer resistance, and the newly developed ice ruler is calibrated for sublimation rate monitoring. Combined with a pseudo-stationary process model, the digital twin enables process development, optimization and control. Using the digital twin, the primary drying conditions were fully dynamically optimized to achieve the fastest drying while ensuring process safety for two different freezing steps: one using a controlled nucleation method to control the ice crystal size, further facilitating process control; and one using a widely applied annealing step. Cost and Global Warming Potential analyses further prove the optimization capability of the digital twin.

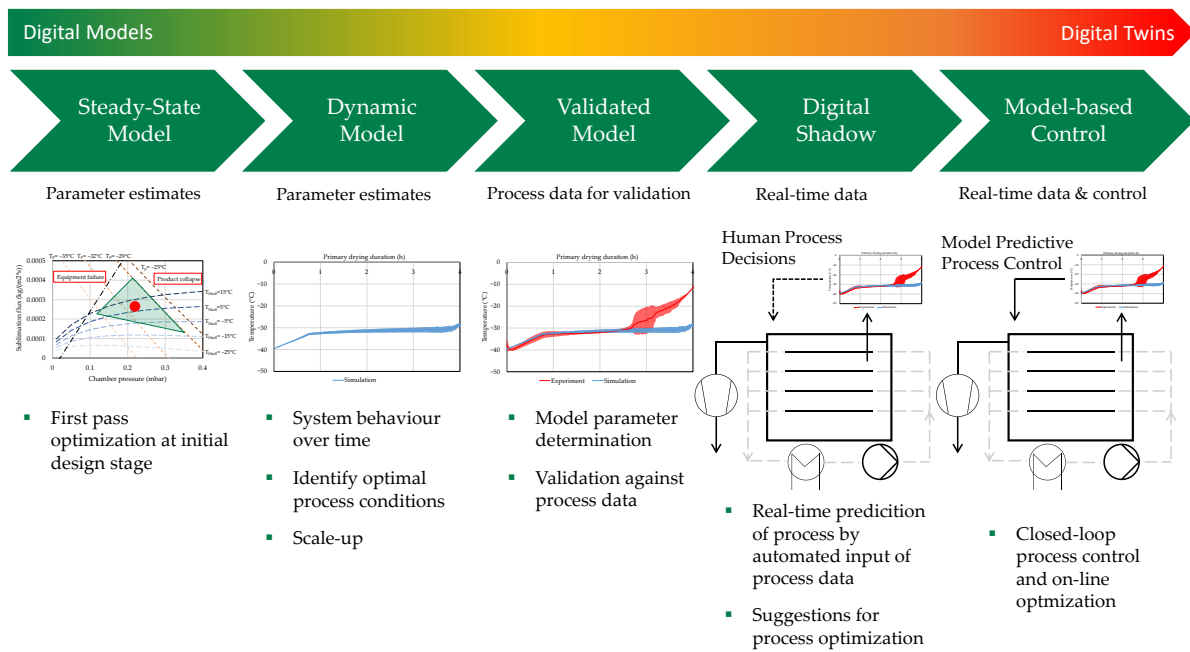


Figure 1. Levels of a digital twin (adopted to lyophilization in accordance with the work of Udugama et al. [85]).

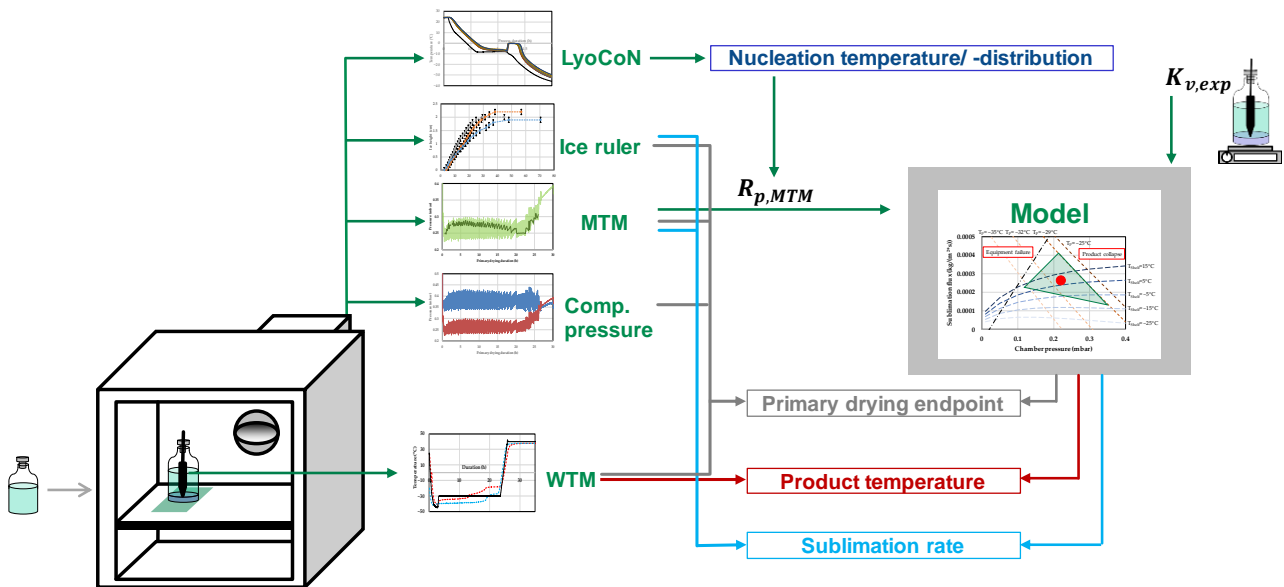


Figure 2. Digital twin for lyophilization processes (adopted from [18]).

2. Materials and Methods

2.1. Product Mixture

Saccharose (d(+)-saccharose (VWR International, Leuven, Belgium)) is dissolved in purified water (arium™ pro, Sartorius AG, Göttingen, Germany) to obtain a 25 g/L solution. The weights are measured using a laboratory scale LC 1200 S balance (Sartorius AG, Göttingen, Germany).

2.2. Freeze-Drying Equipment

The freeze-drying experiments were performed using an Epsilon 2-6D LSCplus pilot freeze-dryer (Martin Christ Gefriertrocknungsanlagen GmbH, Osterode am Harz, Germany). A total of 2 mL of the product solution was filled into 6R injection vials (Martin

Christ Gefriertrocknungsanlagen GmbH, Osterode am Harz, Germany) using an Eppendorf Research[®] plus 0.5–5 mL pipette (Eppendorf AG, Hamburg, Germany). A total of 135 vials were loaded onto the middle shelf of the freeze-dryer. Throughout the freeze-drying process, the product temperature was measured using “Wireless Temperature Measurement plus” (WTMplus) sensors (Martin Christ Gefriertrocknungsanlagen GmbH, Osterode am Harz, Germany) placed centrally on the vial bottom, and the data were recorded using the LPCplus process visualization software (Version 1.5.30.1, Martin Christ Gefriertrocknungsanlagen GmbH, Osterode am Harz, Germany).

2.3. Freeze-Drying Experiments

Two different freezing methods were employed: annealing, and controlled nucleation with the ice fog method LyoCoN (Martin Christ Gefriertrocknungsanlagen GmbH, Osterode am Harz, Germany). The annealing step was adopted from the literature [49]. The shelf temperature is initially decreased to $-45\text{ }^{\circ}\text{C}$ and maintained for 2 h. Subsequently, it is raised to $-20\text{ }^{\circ}\text{C}$ and held for 1 h before returning it to $-45\text{ }^{\circ}\text{C}$ for a final 2 h hold time. The shelf temperature is changed at a rate of $1\text{ }^{\circ}\text{C}/\text{min}$.

The ice fog experiments are conducted using LyoCoN. Initially, the shelf temperature is lowered to the desired nucleation temperature of $-8\text{ }^{\circ}\text{C}$. The samples are allowed to reach equilibrium at the nucleation temperature for a duration of 30 min. Subsequently, the chamber is evacuated to 4 mbar and then aerated to introduce the ice crystals into the chamber. The model is utilized to design an optimal primary drying cycle for both freezing methods. During primary drying, a comparative pressure measurement is implemented as a forwarding condition. The secondary drying phase is conducted at a shelf temperature of $40\text{ }^{\circ}\text{C}$ for 10 h.

2.4. Glass Transition Temperature

A DSC 3 (Mettler-Toledo, Greifensee, Switzerland) is used for the determination of the glass transition temperature. STARe (Mettler-Toledo, Greifensee, Switzerland) is used for documentation and analysis.

2.5. Vial Heat Transfer Coefficient

The vial heat transfer coefficient K_v is determined through ice sublimation tests, which provide individual values for measured vials [90]. In these tests, 6R vials filled with water are loaded onto the shelf. The top and middle shelf are loaded with 135 vials each. Prior to initiating the freeze-drying process, selected vials are weighed. During the primary drying phase, variations in shelf temperature and chamber pressure are implemented. The shelf temperature setpoints are $-25\text{ }^{\circ}\text{C}$, $-12.5\text{ }^{\circ}\text{C}$, and $0\text{ }^{\circ}\text{C}$, while the chamber pressure is set to 0.05 mbar, 0.1 mbar, 0.15 mbar, and 0.3 mbar. After approximately 4 h, the primary drying process is stopped. The selected vials are weighed again following thawing. K_v is calculated using the following equation:

$$K_v = \frac{(\Delta m \cdot \Delta H_{\text{subl}}) / \Delta t}{A_v \cdot (T_s - T_p)} \quad (1)$$

Δm is the measured mass difference, ΔH_{subl} the sublimation enthalpy, Δt the primary drying duration, A_v the outer cross-sectional area of the vial, T_s the shelf temperature, and T_p the product temperature. The product temperature is measured with Wireless Temperature Measurement sensors WTMplus.

2.6. Maximum Allowable Sublimation Flux

The maximum allowable sublimation flux J_{max} that is allowed for the freeze-dryer to ensure pressure control is determined with ice slab tests [91]. Before performing the tests, the K_v of the trays is determined following the same procedure as shown above. A shelf temperature of $0\text{ }^{\circ}\text{C}$ is used and four different pressure setpoints (0.05, 0.1, 0.15 and 0.3 mbar) are used. Three trays filled with 1 L purified water each are loaded onto the three

shelves. During the ice slab tests, the shelf temperature is decreased to $-40\text{ }^{\circ}\text{C}$ and held for 8 h to ensure a full solidification of the water. Then, the chamber is evacuated to the lowest pressure possible for 1.5 h. The setpoints for the shelf temperature are -40 , -30 , -20 , -10 and $0\text{ }^{\circ}\text{C}$, each held for 3 h. During the ice slab test, the chamber pressure, and shelf and product temperature are documented. The calculation of J_{max} is carried out as follows:

$$K_v = K_1 + \frac{K_2 \cdot p_c}{1 + K_3 \cdot p_c} \quad (2)$$

$$J_{max} = \frac{K_v \cdot (T_s - T_p)}{\Delta H_{subl}} \quad (3)$$

K_1 , K_2 and K_3 are constants to fit the equation to experimental data.

2.7. Dry Layer Resistance

The dry layer resistance R_p is determined using an optimized periodic MTMplus (Martin Christ Gefriertrocknungsanlagen GmbH, Osterode am Harz, Germany). The MTMplus measurement is conducted every 10 min and lasts for a maximum of 30 s, depending on the pressure increase. This optimized measurement approach ensures minimal temperature increase in the product, as the measurement is terminated if no pressure rise is detected for 3 s. The MTMplus Analysis software (Version 1.0.0.2, Martin Christ Gefriertrocknungsanlagen GmbH, Osterode am Harz, Germany) is utilized to analyze the data.

2.8. Ice Ruler

The ice ruler is a device comprising a 3D-printed holder with an attached ruler and is affixed to the pipe of the ice condenser. Throughout the freeze-drying process, the ice ruler is monitored using a LyoCam (Martin Christ Gefriertrocknungsanlagen GmbH, Osterode am Harz, Germany) positioned at the sight window of the ice condenser.

2.9. Modeling

A pseudo-stationary model is employed to calculate the endpoint and the product temperature of individual vials during the primary drying phase, taking the coupled heat and mass transfer into account. A detailed derivation of the model can be found elsewhere [70]. The model assumes pseudo-stationary conditions during primary drying, where all heat supplied by the shelf is utilized for sublimation. The accumulation of heat in the frozen and dried regions is disregarded.

$$K_v \cdot (T_s - T_p) \cdot A_v = \frac{\Delta H_{subl}}{R_p} (p_i - p_c) \cdot A_p \quad (4)$$

p_i is the partial vapor pressure on the sublimation interface, p_c is the chamber pressure, and A_p the inner cross-sectional area of the vial.

2.10. Software

Data collection during freeze-drying cycles was performed using LPCplus (Martin Christ Gefriertrocknungsanlagen GmbH, Osterode am Harz, Germany) and the MTM data were analyzed using MTMplus Analysis (Martin Christ Gefriertrocknungsanlagen GmbH, Osterode am Harz, Germany). Thermo-analysis was performed via STARe (Mettler-Toledo, Greifensee, Switzerland). Statistical analysis was carried out using JMP (JMP Inc., SAS Institute, Cary, NC, USA). For the simulations, Aspen Custom Modeler (Aspen Technology Inc., Bedford, MA, USA) was utilized.

3. Results

First, the results of the model parameter determination are shown. Necessary parameters for the model are the vial heat transfer coefficient K_v and the dry layer resistance R_p .

The glass transition temperature and maximum sublimation flux are necessary constraints to ensure product safety during optimization for the used product solution.

3.1. Glass Transition Temperature

The glass transition temperature T_g' has been determined via DSC measurement at -32.6 °C for the saccharose solution used. The high viscosity prevents the flow of the product; therefore, the collapse temperature lays higher at -29 °C [49]. Exceeding this temperature will result in collapse and a structural loss of the product.

3.2. Heat Transfer Coefficient

The heat transfer from the shelf to the product is described by K_v . It can be split into three contributions (direct conduction, gas conduction, and radiation) and it depends on vial type and position, the type of freeze-dryer and process parameters. K_v has been determined for an edge and center vial at two different shelf temperatures and four pressure setpoints. Experiments have been conducted twice. K_v generally increases with the chamber pressure because of an increased gas conduction. At a shelf temperature of -25 °C, the value increases from 18.63 W/m²/K \pm 0.8 W/m²/K (0.05 mbar) to 34.3 W/m²/K \pm 1.6 W/m²/K (0.3 mbar) for an edge vial and from 10.19 W/m²/K \pm 0.18 W/m²/K (0.05 mbar) to 21.94 W/m²/K \pm 0.07 W/m²/K (0.3 mbar). The K_v value of edge vials at this shelf temperature is 56.3 to 84% higher than corresponding center vials values due to increased radiation.

At a shelf temperature of 0 °C, the K_v of edge vials increases from 12.22 W/m²/K \pm 1.04 W/m²/K (0.05 mbar) to 20.18 W/m²/K \pm 2.42 W/m²/K (0.3 mbar). An increase in shelf temperature decreases the edge K_v by 34 to 47%. The center K_v increases from 7.93 W/m²/K \pm 0.1 W/m²/K (0.05 mbar) to 17.87 W/m²/K \pm 3.55 W/m²/K (0.3 mbar). A change of 2.8 to 22% from the center K_v at lower shelf temperature. The deviation between edge and center K_v decreases to a range of 7.6 to 35%.

Next, a statistical analysis was carried out to assess the statistically significant parameters for edge and center K_v . In Figure 3, the evaluation for edge K_v is shown. The p -value is significantly below 0.05, allowing us to determine significant parameters. Two significant parameters could be detected:

- Chamber pressure (+): increased chamber pressure allows for higher gas conduction since more molecules are available to transfer heat.
- Shelf temperature (-): increased shelf temperature lowers the radiation contribution towards K_v , reducing the edge effect.

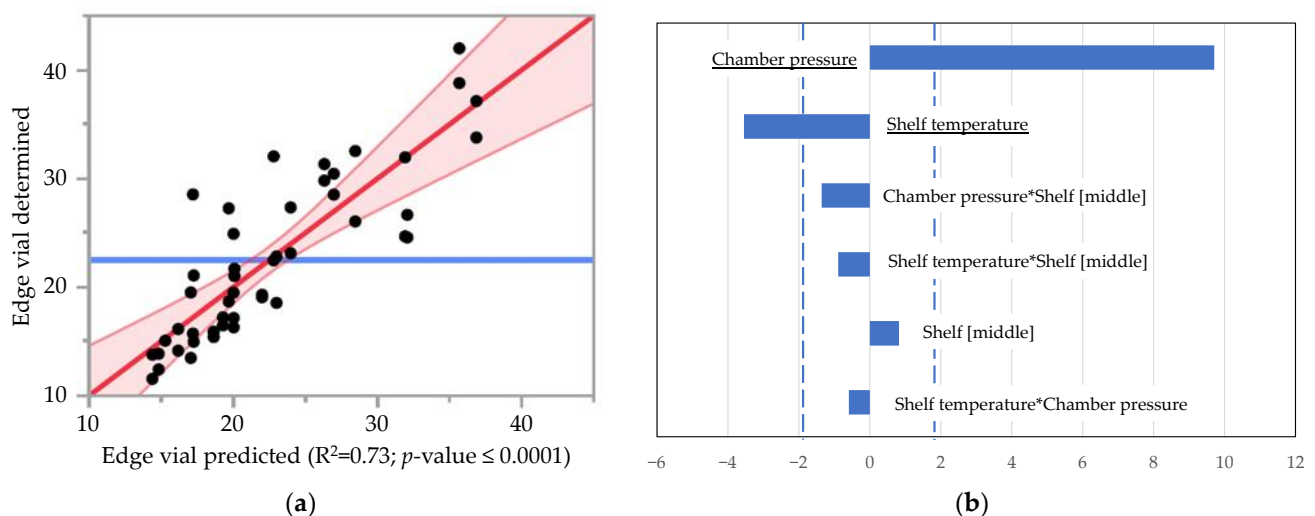


Figure 3. Statistical evaluation for edge vials. (a) Actual-vs-predicted plot (red shadow confidence interval). (b) Pareto diagram of standardized effects (dashed line: significance threshold).

In Figure 4, the statistical evaluation for center K_v is shown. Again, the p -value is significantly below 0.05, allowing us to determine significant parameters. For the center K_v , only the chamber pressure could be identified as significant. An increased chamber pressure allows for increased heat transfer via gas conduction. Center vials are already shielded from radiation; therefore, an increase in shelf temperature leads to no significant change.

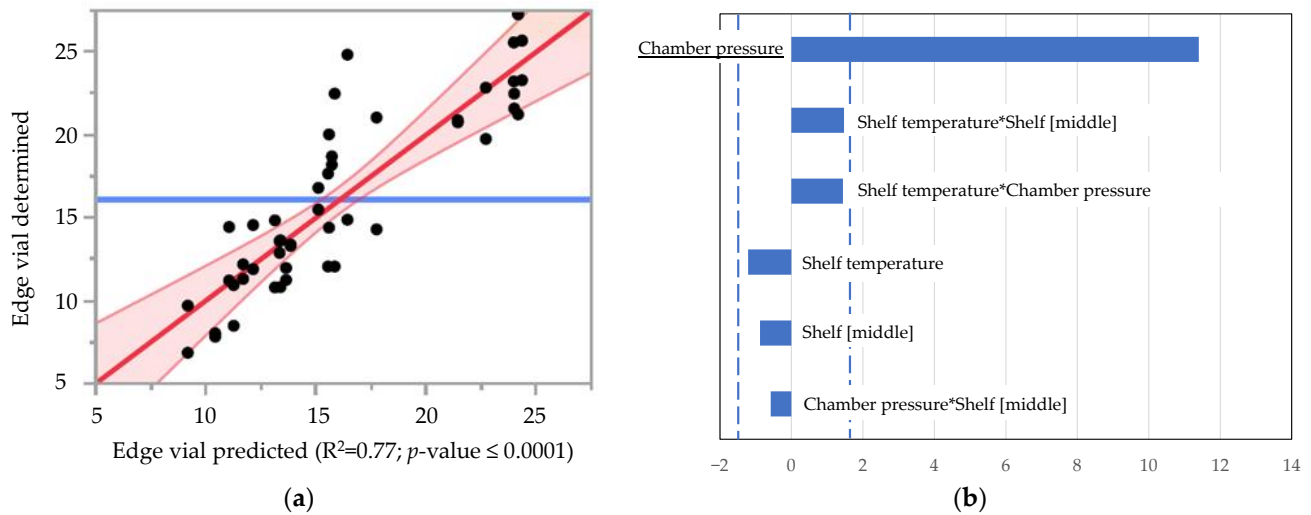


Figure 4. Statistical evaluation for center vial. (a) Actual-vs-predicted plot (red shadow confidence interval). (b) Pareto diagram of standardized effects (dashed line: significance threshold).

3.3. Equipment Constraint

Next, the maximum allowable sublimation flux has to be determined. It presents a second boundary to the process development workflow since exceeding this value will increase the chamber pressure, resulting in the loss of pressure control and an increased product temperature, possibly leading to product loss. To calculate it from the experiments, the K_v of the tray has to be determined first. The results can be seen in Figure A1. K_v increases from $6.54 \text{ W/m}^2/\text{K} \pm 0.34 \text{ W/m}^2/\text{K}$ (0.05 mbar) to $17.6 \text{ W/m}^2/\text{K} \pm 2.18 \text{ W/m}^2/\text{K}$ (0.3 mbar). The parameter from Equation (2) can be determined via the minimization of the square error sum. The calculated and experimentally determined K_v shows a good agreement ($R^2 = 0.99$).

Equation (3) can now be used to calculate the corresponding sublimation flux for the different shelf temperature setpoints and established pressures. The results are shown in Figure A1. At a chamber pressure of $0.046 \text{ mbar} \pm 0.001 \text{ mbar}$, a maximally allowable sublimation flux of $5.7 \times 10^{-5} \text{ kg/m}^2/\text{s} \pm 4.73 \times 10^{-7} \text{ kg/m}^2/\text{s}$ could be determined. The sublimation flux increases to $1.42 \times 10^{-4} \text{ kg/m}^2/\text{s} \pm 2.5 \times 10^{-6} \text{ kg/m}^2/\text{s}$ at a pressure of $0.079 \text{ mbar} \pm 0.006 \text{ mbar}$. A linear regression could be used to describe the experimental results with excellent precision ($R^2 = 0.9985$). During primary drying, it is of the utmost importance to keep the sublimation flux below these critical values to ensure chamber pressure control and product safety.

3.4. Dry Layer Resistance

R_p represents the resistance of the dried layer to the vapor flow. It can be determined using different methods, e.g., TDLAS [56] and pressure rise test [47,50,92]. The dry layer resistances have been determined elsewhere [18,20].

3.5. Optimization

Four parameters are necessary to calibrate the model for the used formulation and equipment (see Figure A2). After the determination of the critical temperature T_c , K_v , J_{max} and R_p , the primary drying process can be simulated regarding primary drying endpoint,

product temperature and sublimation rate. The model can be used for prediction and optimization and/or validation against available experimental data. Since the dependencies of the parameters vary, it is not necessarily required to re-determine all parameters during development. The dependencies are:

- T_c : formulation composition.
- K_p : vial type, freeze-dryer, primary drying process parameters.
- J_{max} : freeze-dryer.
- R_p : formulation composition, freezing process, occurrence of structural changes.

Four different optimization studies were calculated:

- Annealing, optimization for edge vial.
- Annealing, optimization for center vial.
- Controlled nucleation, optimization for edge vial.
- Controlled nucleation, optimization for center vial.

Annealing is often employed in freeze-drying to homogenize the ice crystal structure [93]. Controlled nucleation is used to further explore the optimization potential of controlled nucleation protocols.

The optimized recipes are shown in Figure A3. The optimized shelf temperature profile (black) is shown together with the measured product temperature of a selection of probed vials. For an optimization for an edge vial and freezing with controlled nucleation, the shelf temperature is initially increased to 3.9 °C (annealing: 8.9 °C) and then slowly decreased to −6.2 °C (annealing: −13.8 °C) after 6.1 h (annealing: 7.6 h). An optimization for a center vial leads to an initial shelf temperature of 24.4 °C (annealing: 29.2 °C) and, in the end, to 8.4 °C (annealing: −4.9 °C).

3.6. Dry Layer Resistance

Optimization for the center vial allows for much higher shelf temperatures compared to the usage of edge vials. However, since edge vials generally receive higher radiation energy compared to the center vials, they can be at risk for structural changes or, in the worst case, product collapse. Figure 5 shows the dry layer resistances for the different optimization cases over the dry layer height and the cake appearance of selected lyophilizates after freeze-drying has finished. For both freezing methods, the optimization for the edge vials showed comparable dry layer resistances compared to the reference process. No collapse or structural changes could be detected.

Following freezing with annealing, R_p initially starts at 26,834 m/s ± 7404 m/s with the reference primary drying, then increases to 76,088 m/s ± 38,082 m/s ($L_{dry} = 0.0035$ m), and finally to 113,993 m/s ± 24,635 m/s ($L_{dry} = 0.007$ m). Applying the primary drying conditions for optimization of an edge vial leads to R_p values starting from 29,052 m/s ± 7874 m/s and increasing to 84,676 m/s ± 30,893 m/s ($L_{dry} = 0.0035$ m) and 140,300 m/s ± 53,912 m/s ($L_{dry} = 0.007$ m). R_p deviates 8.27 to 23.08% from the reference value; however, an intact lyophilization cake could be observed. The increase in dry layer resistance is mainly caused by the MTM measurement. It is based on the rise in pressure, and applying more aggressive primary drying conditions leads to an increased R_p compared to slower sublimation processes [52]. An optimization for center vials decreases the R_p up to 53.15%. Here, the primary drying conditions are too aggressive and lead to structural changes in the lyophilized cakes that can be monitored and detected via MTM.

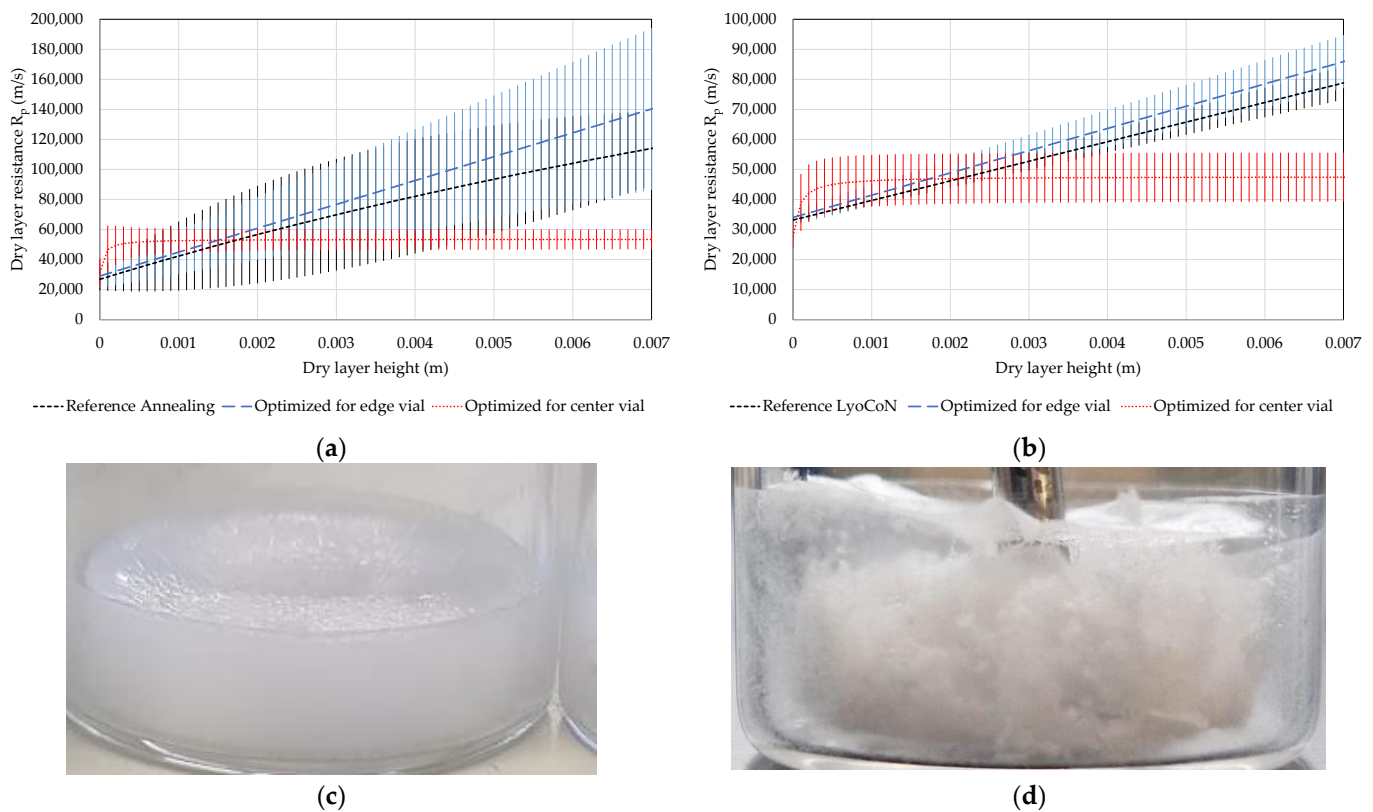


Figure 5. Dry layer resistance, (a) annealing, (b) controlled nucleation, (c) cake appearance annealing optimized for edge vial, (d) cake appearance annealing optimized for center vial.

When applying freezing with LyoCoN, the initial dry layer resistance starts at $33,161 \text{ m/s} \pm 1047 \text{ m/s}$ (reference), $34,037 \text{ m/s} \pm 2632 \text{ m/s}$ (optimization edge vial) and $27,757 \text{ m/s} \pm 3920 \text{ m/s}$ (optimization center vial). R_p for the edge vial optimization deviates 2.64% from the reference, and for the center vial optimization, the deviation is of 16.3%. Increasing the dry layer height increases R_p to $78,819 \text{ m/s} \pm 5546 \text{ m/s}$ (reference), $85,901 \text{ m/s} \pm 8869 \text{ m/s}$ (optimization edge vial) and $47,440 \text{ m/s} \pm 8153 \text{ m/s}$ (optimization center vial), resulting in a deviation of 8.98% (optimization edge vial) or 39.81% (optimization for center vial) compared to the reference. Here, the slight increase in dry layer resistance can also be explained by the increased sublimation rate, and the optimization for a center vial also causes primary drying conditions that lead to structural changes in the cake.

3.7. Product Temperature and Primary Drying Endpoint

Next, the experimentally determined and simulated primary drying product temperature and endpoints for edge and center vials are shown.

At first, the experimental and simulated product temperature and primary drying endpoints for the optimization of an edge vial and annealing are shown in Figure 6. For an edge vial, the product temperature initially increases to $-31 \text{ }^\circ\text{C} \pm 3.9 \text{ }^\circ\text{C}$ and then decreases to $-32.2 \text{ }^\circ\text{C} \pm 4.2 \text{ }^\circ\text{C}$. During the simulation, an average product temperature of $-32.3 \text{ }^\circ\text{C} \pm 2.5 \text{ }^\circ\text{C}$ is predicted. For the center vial, an average product temperature of $-34.9 \text{ }^\circ\text{C} \pm 2.7 \text{ }^\circ\text{C}$ could be experimentally determined and a temperature of $-35.6 \text{ }^\circ\text{C} \pm 1.6 \text{ }^\circ\text{C}$ predicted. Edge vials dry faster and are finished after $6.7 \text{ h} \pm 2.2 \text{ h}$ (simulation: $7.3 \text{ h} \pm 1.5 \text{ h}$), while center vials need $9.4 \text{ h} \pm 2.3 \text{ h}$ (simulation: $9.1 \text{ h} \pm 2 \text{ h}$). The simulation and experiments show good agreement. The forwarding condition, implemented with the PAT comparative pressure measurement, holds the primary drying to a duration to $10.9 \text{ h} \pm 1.2 \text{ h}$, therefore ensuring a safe primary drying duration and removal of all ice before advancing into secondary drying.

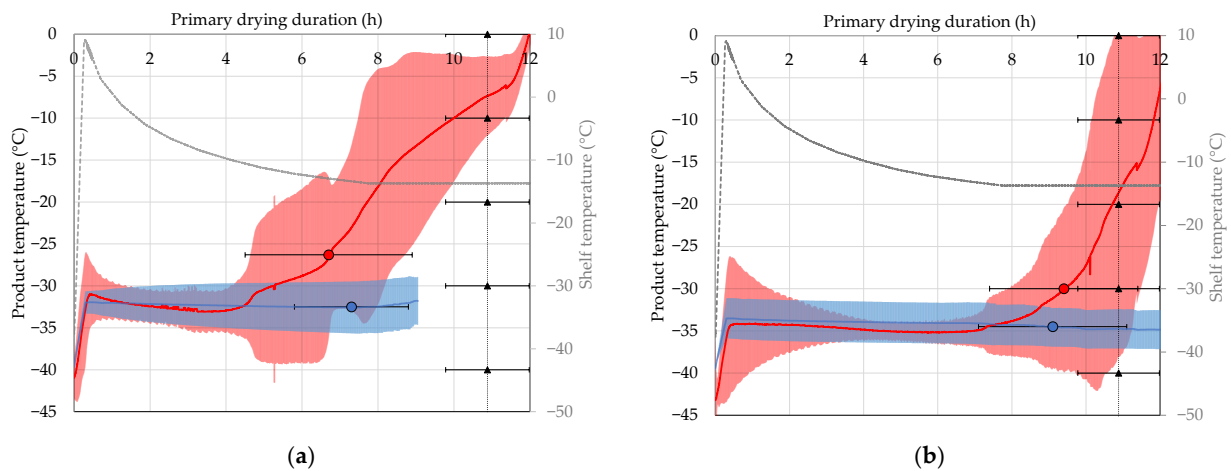


Figure 6. Primary drying endpoint (circle) and product temperature (annealing, optimized for edge vial). (a) Edge vial, (b) center vial (black triangle: forwarding condition, blue: simulation, red: experiment).

Similar results can be found with the implementation of LyoCoN. The resulting experimental and simulated product temperature and primary drying endpoint are shown in Figure 7. For the edge vial, an average product temperature of $-32.4\text{ °C} \pm 1.6\text{ °C}$ could be determined and a temperature of $-32.6\text{ °C} \pm 2.1\text{ °C}$ simulated. The center vial establishes an average primary drying product temperature of $-34.7\text{ °C} \pm 0.8\text{ °C}$ during the experiments and $-34\text{ °C} \pm 2.4\text{ °C}$ during simulation. The forwarding conditions also ensure a safe primary drying process by prolonging the primary drying duration to $9.7\text{ h} \pm 0.7\text{ h}$. During this period, the edge (experiment: $5.6\text{ h} \pm 0.9\text{ h}$, simulation: $5.9\text{ h} \pm 1.4\text{ h}$) and center vials (experiment: $8.3\text{ h} \pm 0.9\text{ h}$, simulation: $8\text{ h} \pm 1.3\text{ h}$) are finished.

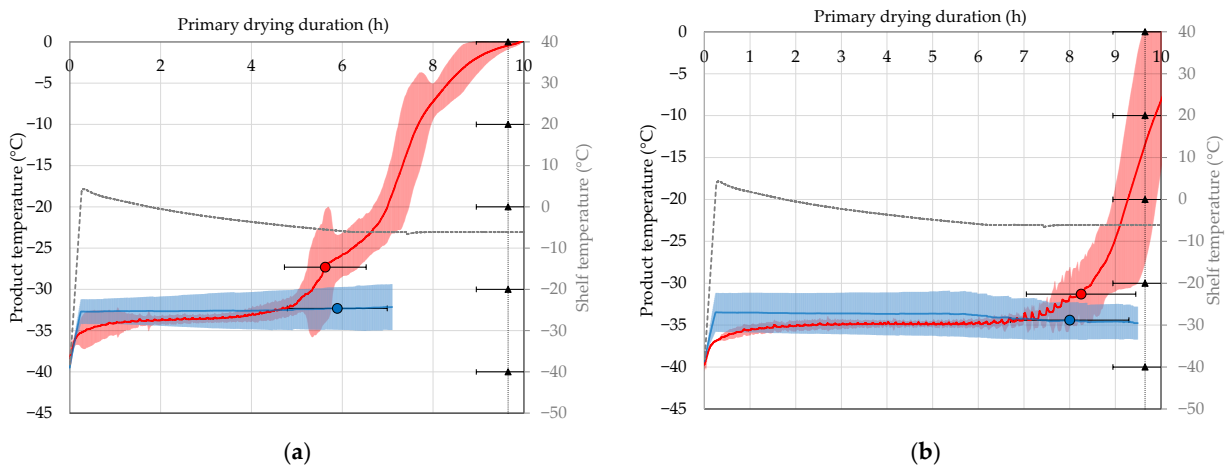


Figure 7. Primary drying endpoint (circle) and product temperature (LyoCoN, optimized for edge vial). (a) Edge vial, (b) center vial (black triangle: forwarding condition, blue: simulation, red: experiment).

Next, the resulting product temperature profiles and primary drying endpoints are shown for the optimization of the center vials. Figure 8 shows the results for the annealing process. The edge vials dry at an average product temperature of $-31.3\text{ °C} \pm 4.4\text{ °C}$. This exceeds the collapse temperature of the solution, and therefore structural changes will occur that can be detected via MTM as an alteration in the dry layer resistance. Since the shelf temperature is lowered, no complete structural loss is observed. The simulations showed an average product temperature of $-31.3\text{ °C} \pm 4\text{ °C}$ and are in good agreement with the experiments. The center vials dry at a lower product temperature of $-33.4\text{ °C} \pm 3.2\text{ °C}$ than edge vials because they receive less radiative energy. However, structural changes also occur here. The simulated product temperature establishes a value of $-32.3\text{ °C} \pm 5\text{ °C}$,

confirming the values of the experiment. Increasing the shelf temperature by optimizing the primary drying for center vials increases the product temperature for edge vials by 3.5% (simulation: 4%) and by 3.9% (simulations: 4.9%), resulting in structural changes.

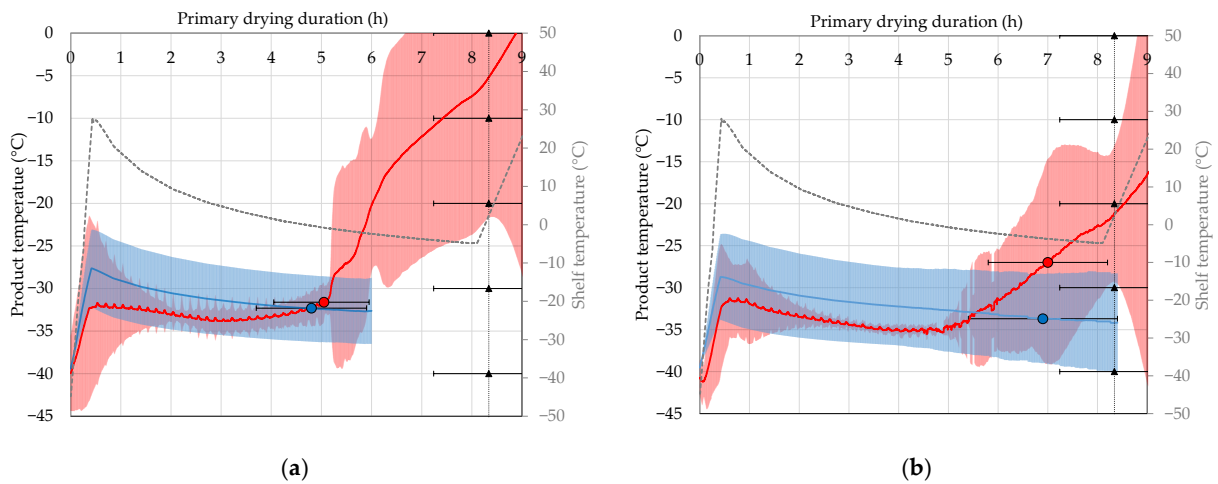


Figure 8. Primary drying endpoint (circle) and product temperature (annealing, optimized for center vial). (a) Edge vial, (b) center vial (black triangle: forwarding condition, blue: simulation, red: experiment).

However, the forwarding condition still maintains a safe process duration regarding the removal of ice. No complete loss due to too early advancement to secondary drying could be detected. The primary drying endpoint has been detected through comparative pressure measurement at $8.3 \text{ h} \pm 1.1 \text{ h}$, giving the edge (experiment: $5.05 \text{ h} \pm 0.9 \text{ h}$, simulation: $4.8 \text{ h} \pm 1.3 \text{ h}$) and center vials (experiment: $7 \text{ h} \pm 1.2 \text{ h}$, simulation: $6.9 \text{ h} \pm 1.5 \text{ h}$) enough time for primary drying. Although structural changes occurred, the simulations were able to predict the experiments well.

The same results regarding structural changes and agreement between the experiment and simulation could be found when employing controlled nucleation in the freezing step (see Figure 9). For the edge vials, an average temperature of $-31.2 \text{ }^\circ\text{C} \pm 1.7 \text{ }^\circ\text{C}$ could be measured and a temperature of $-29.8 \text{ }^\circ\text{C} \pm 3.9 \text{ }^\circ\text{C}$ predicted. The product temperature decreases to $-32.8 \text{ }^\circ\text{C} \pm 0.7 \text{ }^\circ\text{C}$ (simulation: $-34 \text{ }^\circ\text{C} \pm 1.9 \text{ }^\circ\text{C}$) for the center vials. The simulated and experimentally determined product temperatures show good agreement even though structural changes could be detected.

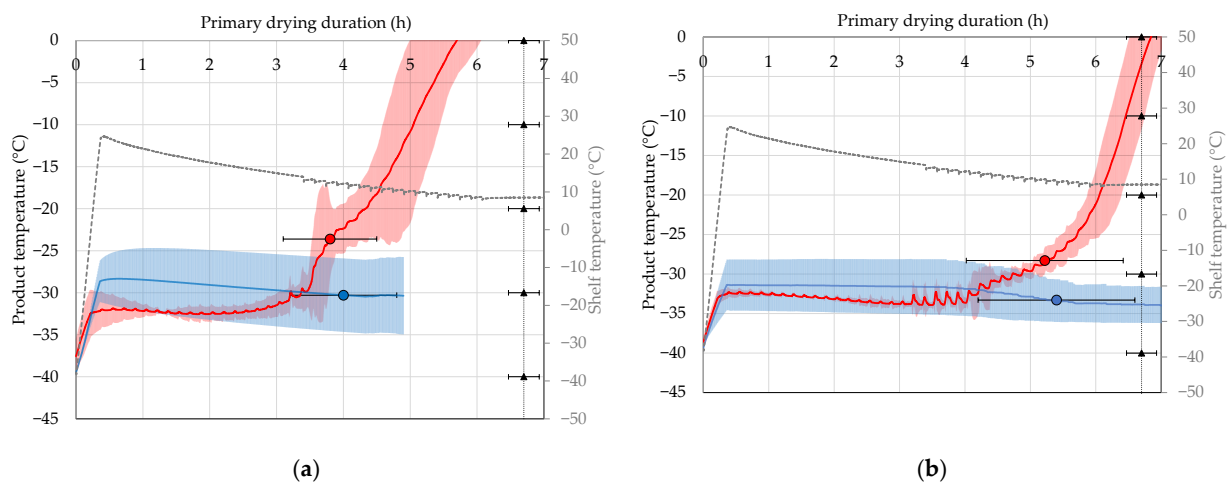


Figure 9. Primary drying endpoint (circle) and product temperature (LyoCoN, optimized for center vial). (a) Edge vial, (b) center vial (black triangle: forwarding condition, blue: simulation, red: experiment).

3.8. Sublimation Rate

The control and prediction of the sublimation rate is important to ensure product safety. In this study, the sublimed ice mass is determined via MTM, process model and the ice ruler. The ice ruler has already been introduced [89]. Here, the ice height on the ice condenser needs to be calibrated to a mass value.

The sublimed water amount is plotted against the corresponding ice ruler height to describe the relationship between them (see Figure A4). Experiments are carried out twice. Next to the measurement points, some ice ruler pictures are depicted to see the height increase. A fill quantity of 100 g water results in an ice height of $0.58 \text{ cm} \pm 0.25 \text{ cm}$. Doubling the fill quantity to 200 g increases the ice height to $0.8 \text{ cm} \pm 0.1 \text{ cm}$. The other ice heights for the different fill quantities are as follows: $1.55 \text{ cm} \pm 0.1 \text{ cm}$ (500 g), $2.55 \text{ cm} \pm 0.12 \text{ cm}$ (750 g) and $3.05 \text{ cm} \pm 0.29 \text{ cm}$ (1000 g). A linear regression through the zero point is used to describe the experimentally determined water amount over ice height. The determination coefficient is 0.98; therefore, a very good agreement between the experiment and the correlation could be achieved.

The sublimed ice mass profiles for ice ruler, simulation, MTM and experimental determination for both optimization protocols are shown in Figure 10. To determine the experimental value, the primary drying is aborted at the desired time point, the samples are allowed to thaw, and the mass difference is determined.

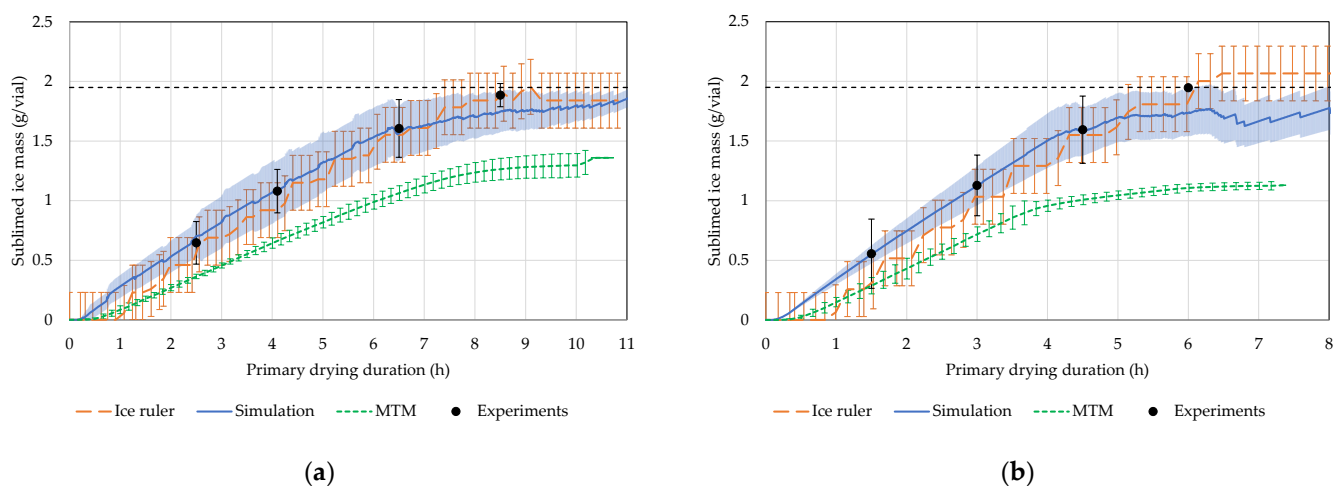


Figure 10. Sublimed ice mass over primary drying duration, (a) LyoCoN, optimization for edge vial, (b) LyoCoN, optimization for center vial.

The primary drying endpoint of the optimized process for the edge vial is determined at $9.9 \text{ h} \pm 0.66 \text{ h}$ with the ice ruler, $10 \text{ h} \pm 1.3 \text{ h}$ with the simulation, and $9.6 \text{ h} \pm 0.6 \text{ h}$ with MTM. After 2.5 h, the ice ruler shows a sublimed ice mass of $0.63 \text{ g/vial} \pm 0.23 \text{ g/vial}$, while the simulation and MTM determine $0.7 \text{ g/vial} \pm 0.17 \text{ g/vial}$ and $0.36 \text{ g/vial} \pm 0.02 \text{ g/vial}$. The ice ruler and simulation deviate by 3.1 or 7.7% from the experimentally determined $0.65 \text{ g/vial} \pm 0.18 \text{ g/vial}$, while MTM deviates by 44.6%. Throughout the primary drying process, the sublimed ice mass increases from $1.08 \text{ g/vial} \pm 0.18 \text{ g/vial}$ (4.1 h, experiments) to $1.61 \text{ g/vial} \pm 0.24 \text{ g/vial}$ (6.5 h, experiments) and finally to $1.89 \text{ g/vial} \pm 0.1 \text{ g/vial}$ (8.5 h, experiments). The ice ruler deviates between 0 and 14.8%, the simulation from 0 to 7.4%, and MTM from 33.3 to 44.6% from the experimentally determined values, showcasing the efficiency of ice ruler and simulation to determine the sublimed ice mass.

The results for the optimized process for the center vial are similar. After 1.5 h primary drying time, the ice ruler shows a sublimed ice mass per vial of $0.32 \text{ g/vial} \pm 0.23 \text{ g/vial}$ (simulation: $0.55 \text{ g/vial} \pm 0.08 \text{ g/vial}$, MTM: $0.29 \text{ g/vial} \pm 0.07 \text{ g/vial}$), causing a deviation of 45.8% for the ice ruler, 6.8% for the simulation and 50.8% for MTM compared to the experimental value of $0.56 \text{ g/vial} \pm 0.29 \text{ g/vial}$. These values increase to 1.81 g/vial

± 0.23 g/vial (ice ruler), 1.74 g/vial ± 0.19 g/vial (simulation) and 1.11 g/vial ± 0.05 g/vial (MTM) after 6 h. The ice ruler deviates 2.5 to 8.8%, the simulation 0 to 10.3% and MTM 36.3 to 42.8% from the experimentally determined values. Primary drying is finished after 6.4 h ± 0.4 h (ice ruler), 6.5 ± 1.19 h (simulation) and 6.7 h ± 0.22 h (MTM).

3.9. Cycle Time Reduction

The optimization of the primary drying conditions leads to a shortened cycle time, increasing productivity while maintaining product safety. Since the optimization for the center vials leads to changes in the products' structure, only the cases of optimization for the edge vial are compared with the reference. As the reference process, the protocol of Lewis et al. has been chosen, which uses annealing for freezing [49]. In Table 1, the cycle times for the different protocols are shown. In all protocols, the same secondary drying and downtime for unloading, defrosting and preparations are used.

Table 1. Cycle times (value in brackets stand for the reduction based on the reference duration).

	Reference Annealing	Optimization LyoCoN	Optimization Annealing
Freezing duration	6:55	3:20 (49%)	6:55 (0%)
Primary drying duration	50:00	9:40 (81%)	11:00 (78%)
Secondary drying duration	11:00	11:00 (0%)	11:00 (0%)
Downtime	4:00	4:00 (0%)	4:00 (0%)
Total process time	72:00	28:00 (61%)	33:00 (54%)

Compared to the reference process, the application of LyoCoN reduces the freezing duration by 49% from 6.92 h to 3.33 h. More drastic changes are seen in the primary drying duration. The reference process has a primary drying duration of 50 h. The optimization of the primary drying conditions for the annealing freezing protocol decreases the primary drying duration by 78% to 11 h. The application of LyoCoN further shortens the primary drying time to 9.67 h, leading to a reduction of 81% compared to the reference and 12% to the optimized reference process. The total cycle time can be reduced by 54% (optimization annealing) and 61% (optimization LyoCoN) compared to the reference process.

Substituting annealing with a controlled nucleation process step leads to a further reduction of 15% in total process duration. The decreased cycle time leads to an increased productivity (see Figure A5). During a 5-day working week, the reference process can only be carried out once, while the optimized annealing process allows for three and the optimized LyoCoN process for four cycles, increasing the productivity by 200 or 300%. Compared to the optimized annealing protocol, the implementation of controlled nucleation increases the productivity by 33%. During a 7-day working week, 2.3 cycles of the reference, 5.1 of the optimized annealing and 6 of the optimized LyoCoN cycles can be finished, increasing the productivity by 118% (optimized annealing) or 157% (optimized LyoCoN). The implementation of controlled nucleation allows for a productivity increase of 18% compared to the optimized annealing process step.

3.10. Cost Analysis

Next, a cost analysis was carried out with the model of Stratta et al. [94]. Freeze-dryer equipment parameters from these authors have been used for estimation of the costs together with the cycle conditions developed here. The Cost of Goods (COGs) for the different cycles for 5- and 7-day working weeks are shown in Table 2. For the reference annealing process, a COG of 70 EUR/kg_{product} with a 5-day and 32 EUR/kg_{product} for a 7-day working week are calculated. A switch to a 7-day working week reduces the COG by 54%, caused by the increased cycles per week reducing the share of Capital Costs (CC) on the Total Costs (TC) from 94 to 87%. As Stratta et al. mentioned, the COG of freeze-dried products can be lowered most efficiently by incorporating more cycles into the lifecycle of a freeze-dryer [94]. Optimizing the primary drying of the annealing process reduces

the COG for a 5-day working week by 66% to 24 EUR/kg_{product} and for a 7-day working week by 55% to 15 EUR/kg_{product}. Incorporating controlled nucleation further reduces the COG for a 5-day working week by 24% compared to the optimized annealing process (75% compared to the reference annealing process) and by 15% (60% compared to the reference annealing process) for a 7-day working week to 13 EUR/kg_{product}.

Table 2. Cost of Goods (COG) for different cycles (value in brackets stands for the reduction based on the reference).

		Reference Annealing	Optimization LyoCoN	Optimization Annealing
COG (5 days)	EUR/kg _{product}	70	18	24
	EUR/Vial	0.14	0.036 (75%)	0.047 (66%)
COG (7 days)	EUR/kg _{product}	32	13	15
	EUR/Vial	0.064	0.025 (60%)	0.029 (55%)

The optimization of the primary drying conditions decreases the share of operational costs of this phase from 78% to 48% (53% with controlled nucleation), showing that the optimized processes increase the primary drying efficiency. The increased efficiency of the process leads to a reduction in energy consumption and carbon footprint via a reduction in the Global Warming Potential (GWP) between 49 and 64% (see Figure 11).

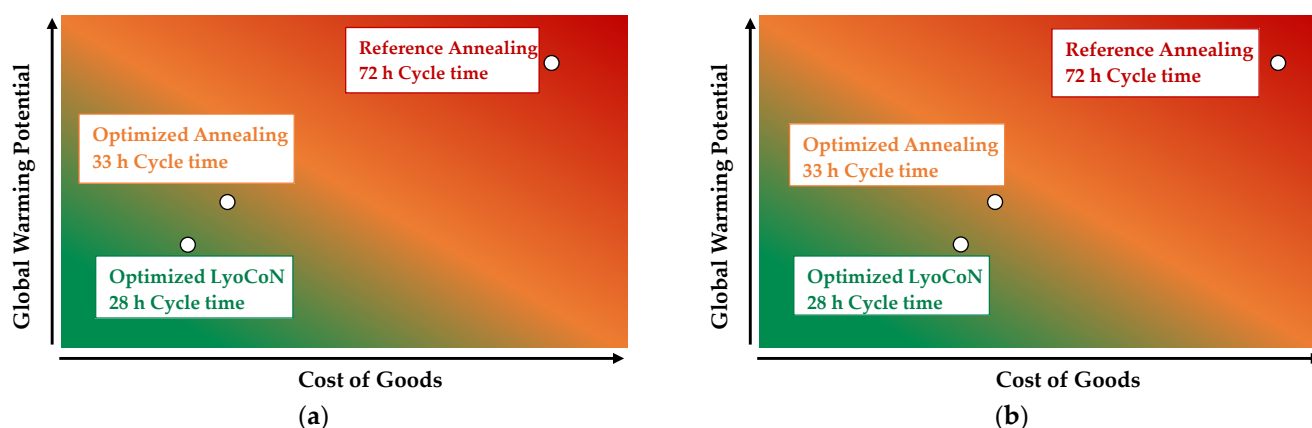


Figure 11. GWP vs. COG for different process scenarios (a) 5-day working week, (b) 7-day working week.

4. Discussion

In this study, a digital twin has been validated for process optimization and control for a sucrose-based example system. The digital twin consists of a process model and PAT-tools to adopt the model status to time-dependent process reality. Controlled nucleation is used to control the ice crystal size in the freezing step, while comparative pressure measurement, MTM and ice ruler are used to gather distinct information during primary drying to incorporate them into the process model, allowing for a forecast of the process conditions. To establish a digital twin, several parameters need to be determined beforehand: the critical temperature of the formulation, the maximum allowable sublimation flux of the freeze-dryer, the vial heat transfer coefficient, and the dry layer resistance.

During primary drying, it is of the utmost importance to keep the product's temperature under the critical temperature of the formulation. T_g' for sucrose has been determined via DSC at -32.6 °C.

The maximum allowable sublimation flux has been determined through ice slab tests. At a chamber pressure of $0.046 \text{ mbar} \pm 0.001 \text{ mbar}$, a maximally allowable sublimation flux of $5.7 \times 10^{-5} \text{ kg/m}^2/\text{s} \pm 4.73 \times 10^{-7} \text{ kg/m}^2/\text{s}$ could be determined that increases to

$1.42 \times 10^{-4} \text{ kg/m}^2/\text{s} \pm 2.5 \times 10^{-6} \text{ kg/m}^2/\text{s}$ at a pressure of $0.079 \text{ mbar} \pm 0.006 \text{ mbar}$. The experimental data can be excellently described through a linear regression ($R^2 = 0.9985$).

The vial heat transfer coefficient is determined via ice sublimation tests for distinct vials. The edge vials have a 7.6 to 84% higher K_v , ranging from $12.22 \text{ W/m}^2/\text{K} \pm 1.04 \text{ W/m}^2/\text{K}$ to $34.3 \text{ W/m}^2/\text{K} \pm 1.6 \text{ W/m}^2/\text{K}$, than the center vials ($7.93 \text{ W/m}^2/\text{K} \pm 0.1 \text{ W/m}^2/\text{K}$ to $21.94 \text{ W/m}^2/\text{K} \pm 0.07 \text{ W/m}^2/\text{K}$), which is caused by increased radiation and nesting effects. They also show different statistical significances. For the edge vials, the shelf temperature negatively correlates and the chamber pressure positively correlates with the K_v values, while for the center vials, the chamber pressure is the only significant parameter. The dry layer resistance is determined online via MTM.

Gathering all these parameters allows for the model-based optimization of the primary drying for the used formulation. Four optimization studies have been tested:

- Annealing, optimization for edge vial.
- Annealing, optimization for center vial.
- LyoCoN, optimization for edge vial.
- LyoCoN, optimization for center vial.

LyoCoN is implemented to establish a controlled nucleation approach resulting in more control of the digital twin, while annealing is commonly used in freezing processes. The resulting shelf temperature is at first increased to values between 3.9 and $29.2 \text{ }^\circ\text{C}$, and is then asymptotically lowered to values ranging from -4.9 to $8.4 \text{ }^\circ\text{C}$ depending on the optimization case.

These have been experimentally investigated to validate the digital twin. The results for the product temperatures are summarized in Table 3. The simulation and experiments are in good agreement. The mean value deviates between 0.16 and 4.73% , which is smaller than the experimental errors of 4.64% to 14.93% .

Table 3. Determined and calculated average product temperature of edge and center vials (simulation results in brackets).

Freezing Method	Primary Drying	Primary Drying Product Temperature ($^\circ\text{C}$)	
		Edge	Center
LyoCoN	Optimization edge vial	-32.4 ± 1.6 (-32.6 ± 2.1)	-34.7 ± 0.8 (-34 ± 2.4)
	Optimization center vial	-31.2 ± 1.7 (-29.8 ± 3.9)	-32.8 ± 0.7 (-34 ± 1.9)
Annealing	Optimization edge vial	-32 ± 4.2 (-32.3 ± 2.5)	-34.9 ± 2.7 (-35.6 ± 1.6)
	Optimization center vial	-31.3 ± 4.4 (-31.3 ± 4)	-33.4 ± 3.2 (-32.3 ± 5)

The edge vials dry at a temperature between $1.5 \text{ }^\circ\text{C}$ and $2.9 \text{ }^\circ\text{C}$ (about 5% to 9%) hotter than that of the center vials. Therefore, a rigorous optimization for the center vials increases the product temperature of the warmer vials over the critical product temperature, causing structural changes. This could be evidenced with the dry layer resistance and through a visual inspection of the lyophilized cakes.

The dry layer resistances are summarized in Table 4. An optimization for the edge vials with annealing leads to a deviation of 8 to 23% of the dry layer from the reference process, while an optimization of the center vials leads to 53% change caused by structural damage of the lyophilizate. Employing a controlled nucleation method leads to a deviation of R_p of 9% for the optimization for the edge vials, and of 40% for the optimization of the center vials.

Table 4. Dry layer resistances for different freezing and primary drying conditions at selected dry layer heights.

Freezing Method	Primary Drying	Dry Layer Resistance (m/s)		
		$L_{dry} = 0$ m	$L_{dry} = 0.0035$ m	$L_{dry} = 0.007$ m
LyoCoN	Reference	33,161 ± 1047	55,990 ± 3296	78,819 ± 5546
	Optimization edge vial	34,037 ± 2632	59,969 ± 5751	85,901 ± 8869
	Optimization center vial	27,757 ± 3920	47,228 ± 8245	47,440 ± 8153
Annealing	Reference	26,834 ± 7404	76,088 ± 38,082	113,993 ± 24,635
	Optimization edge vial	29,052 ± 7874	84,676 ± 30,893	140,300 ± 53,912
	Optimization center vial	31,448 ± 9295	53,263 ± 6859	53,404 ± 6586

The primary drying endpoint is critical for maintaining a safe process while increasing the productivity of the freeze-drying cycle. The endpoints are summarized in Table 5. Since the edge vials dry at a hotter temperature, their primary drying is finished 1.4 to 2.6 h earlier than that of the center vials, leading to deviations of 37 to 46.5% between these two vial classes. The simulations can predict the primary drying endpoint with a deviation of 1.5% to 8%, which is smaller than the experimental error of 10.9 to 32%. The forwarding condition implemented using comparative pressure measurement increases the duration of the primary drying process based on real-time data, leading to a safe primary drying duration that is increased between 14% and 16% compared to the center vial value.

Table 5. Determined and simulated primary drying endpoints for distinct vials and forwarding condition (brackets: simulation results).

Freezing Method	Primary Drying	Primary Drying Endpoint (h)		
		Edge	Center	Forwarding
LyoCoN	Optimization edge vial	5.63 ± 0.9 (5.9 ± 1.4)	8.25 ± 0.9 (8 ± 1.3)	9.65 ± 0.7
	Optimization center vial	3.8 ± 0.5 (4 ± 0.8)	5.2 ± 1.3 (5.4 ± 1.3)	6.7 ± 0.3
Annealing	Optimization edge vial	6.7 ± 2.2 (7.3 ± 1.5)	9.4 h ± 2.3 (9.1 ± 2)	10.88 ± 1.15
	Optimization center vial	5.05 ± 0.9 (4.8 ± 1.3)	7 ± 1.2 (6.9 ± 1.5)	8.3 ± 1.1

Besides the product temperature, the sublimed ice mass can also be monitored using the digital twin. The results are summarized in Table 6. The ice ruler and simulation show small deviations compared to the experimental values. The deviations for the ice ruler range from 0 to 14.8%, and for the simulation, from 0 to 10.3%, which is smaller than the experimental error ranging from 5 to 49%, showcasing the precision of the digital twin.

Next, the process optimization potential of the digital twin is assessed. Here, only the optimization of the edge vial cases has been evaluated because no structural changes could be detected.

A literature process has been used as a reference that uses annealing during freezing [49]. Employing primary drying optimization in this process results in a cycle reduction of 39 h (54%). Implementing controlled nucleation allows for further optimization of the primary drying and freezing step, leading to a further shortening of 15% to 61% compared to the reference. For a 5-day working week, the productivity of the digital twin incorporating control of freezing and primary drying increases by 300% (5-day week), and by 157% for a 7-day working week compared to the reference process. This drastic cycle shortening

results in a cost reduction of 75% (5-day week) or 60% (7-day week) compared to the reference process, and a 24% (5-day week) or 14.6% (7-day week) reduction in comparison to the optimized reference process.

Table 6. Sublimed ice mass of the two optimization cases with controlled nucleation.

Primary Drying	Timepoint (h)	Ice Ruler	Sublimed Ice Mass (g/vial)		
			Simulation	MTM	Experiments
Optimization edge vial	2.5	0.63 ± 0.23	0.7 ± 0.17	0.36 ± 0.02	0.65 ± 0.18
	4.1	0.92 ± 0.23	1.08 ± 0.25	0.68 ± 0.05	1.08 ± 0.18
	6.5	1.55 ± 0.23	1.56 ± 0.23	1.06 ± 0.06	1.61 ± 0.24
	8.5	1.89 ± 0.23	1.75 ± 0.17	1.26 ± 0.09	1.89 ± 0.1
Optimization center vial	1.5	0.32 ± 0.23	0.55 ± 0.08	0.29 ± 0.07	0.56 ± 0.29
	3	1.03 ± 0.23	1.12 ± 0.16	0.72 ± 0.06	1.13 ± 0.25
	4.5	1.55 ± 0.23	1.59 ± 0.21	1.01 ± 0.04	1.59 ± 0.28
	6	1.81 ± 0.23	1.74 ± 0.19	1.11 ± 0.05	1.94 ± 0.01

5. Conclusions and Recommendations

The time required for cycle development depends on several factors: product complexity, the experience and knowledge of the development team, and availability of resources. The development process typically involves a series of experiments, like trial runs, iterative adjustments or Design of Experiments, making it labor and time consuming, requiring a time of development ranging from weeks up to several months.

Implementing QbD with a digital twin can accelerate this development process by providing a strong science-based foundation that emphasizes process understanding and risk assessment.

First, appropriate freezing methods have to be established. Controlled nucleation is recommended as it can facilitate the freezing design by enhancing process consistency and reproducibility. Here, the Design of Experiments with different nucleation temperatures and post-nucleation holds should be tested with a low amount of product to establish the freezing step for the formulation.

The primary drying optimization follows. For the model-based optimization, four parameters are necessary:

- Critical temperature T_c of the formulation: The critical temperature of the formulation should be characterized during formulation development with DSC or Freeze-Drying Microscopy (FDM), and the maximum allowable sublimation flux of the freeze-dryer should be determined beforehand during equipment qualification because they are the two constraints of the primary drying design space.
- Vial heat transfer coefficient K_v : This study showed the different behavior of edge and center K_v depending on the process conditions. Since process optimization yields high shelf temperatures, the authors recommend determining the K_v of distinct edge and center vials at a shelf temperature of 0 °C. Three pressure setpoints are necessary to describe the pressure dependency of K_v . An ice sublimation test only requires water and takes one day. The duration of K_v tests can be calculated as follows: 1 day*Number of pressure setpoints × repetition. In this study, four pressure set points have been determined twice, resulting in 8 days of work.
- Maximum allowable sublimation flux J_{max} : In this study, ice slab tests have been used for equipment qualification. With increasing chamber pressure, the freeze-dryer allows for higher sublimation rates while maintaining pressure control. This needs to be carried out once and requires around 5 working days.
- Dry layer resistance R_p : In this study, we used two experiments with a partial load (one fully loaded shelf), controlled nucleation and more optimized primary drying conditions to determine it. A total of 540 mL product solutions have been used (135 vials × 2 mL/vial × 2 experiments) and 5 working days were needed.

For model-based optimization, the target temperature was set 3 °C below the critical temperature (if only center K_v is known, a target temperature of 5–6 °C lower than T_c should be utilized to prevent the collapse of the hotter vials). The simulations were finished and analyzed in one working day.

In total, 14 working days and a 540 mL product solution were necessary to develop optimized and robust primary drying conditions for the given formulation with the introduced digital twin. For a new formulation in the same vial, only the dry layer resistance and critical temperature have to be determined, resulting in a total of only 5 days. For a new formulation in a new primary container, the whole workflow has to be repeated.

In this study, a digital twin approach for process optimization and process control is validated. A pseudo-stationary process model is used to predict the product temperature and optimize the primary drying conditions. The experiments and the simulation are in good agreement. A comparative pressure measurement, MTM and ice ruler are used to measure critical process parameters during primary drying and allow for the adoption of the digital twin status to reality. Applying the digital twin significantly reduces the workload of designing optimized and robust primary drying conditions from several weeks to 14 days while consuming small amounts of product solution. Implementing a controlled nucleation method into the digital twin further deepens the process control and allows for a 160% to 300% increase in productivity while maintaining a safe process, leading to a cost reduction of 60–75% based on the working schedule described.

Author Contributions: A.J. performed experiments, modeling and simulation, and wrote this paper. P.K. and F.H. assisted with laboratory and piloting equipment, as well as with expert knowledge regarding operations and objectives. J.S. was responsible for conception and supervision. All authors have read and agreed to the published version of the manuscript.

Funding: This research was funded by the Bundesministerium für Wirtschaft und Klimaschutz (BMWK) under grant number 03EN2067D. The authors especially thank M. Gahr (Projekträger FZ Jülich) for funding this scientific work.

Data Availability Statement: Data are contained within the article.

Acknowledgments: We gratefully acknowledge the support of P. Knerr and F. Harms from Martin Christ Gefriertrocknungsanlagen GmbH for kindly providing the Epsilon 2-6D LSCplus, as well as ongoing advice and support. The authors acknowledge support by the Open Access Publishing Fund of Clausthal University of Technology.

Conflicts of Interest: Alex Juckers, Petra Knerr and Frank Harms are employed by the company Martin Christ Gefriertrocknungsanlagen GmbH. The remaining author declare that the research was conducted in the absence of any commercial or financial relationships that could be construed as a potential conflict of interest.

Appendix A

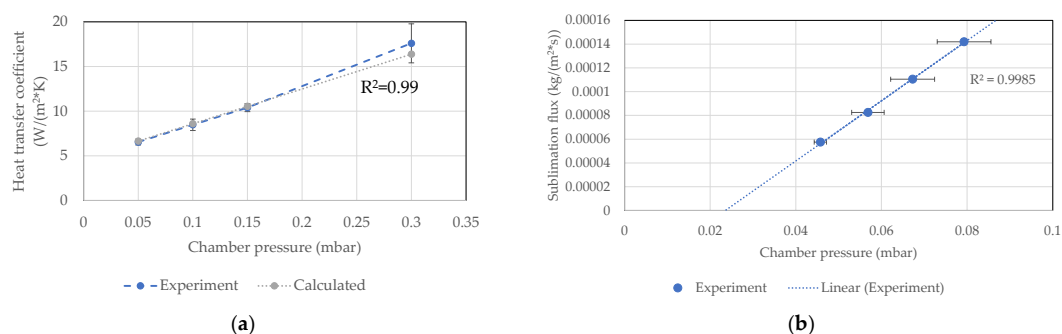


Figure A1. (a) K_v over chamber pressure for tray. (b) Sublimation flux over chamber pressure.

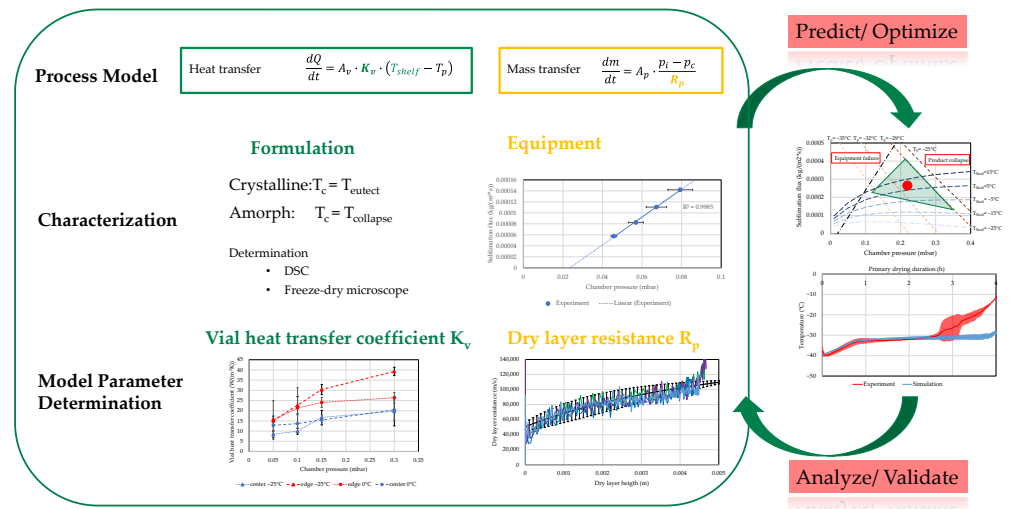


Figure A2. Workflow for model-based optimization and validation of primary drying processes.

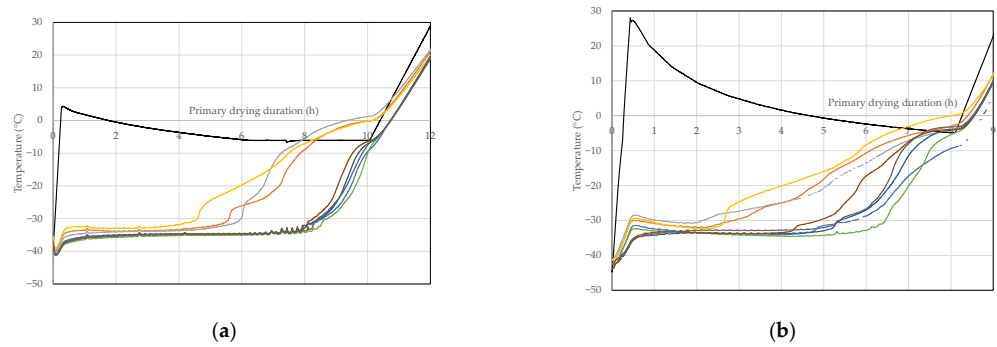


Figure A3. Optimized shelf temperature profiles (black: shelf temperature, color: product temperature). (a) Controlled nucleation, optimized for edge vial. (b) Annealing, optimized for center vial.

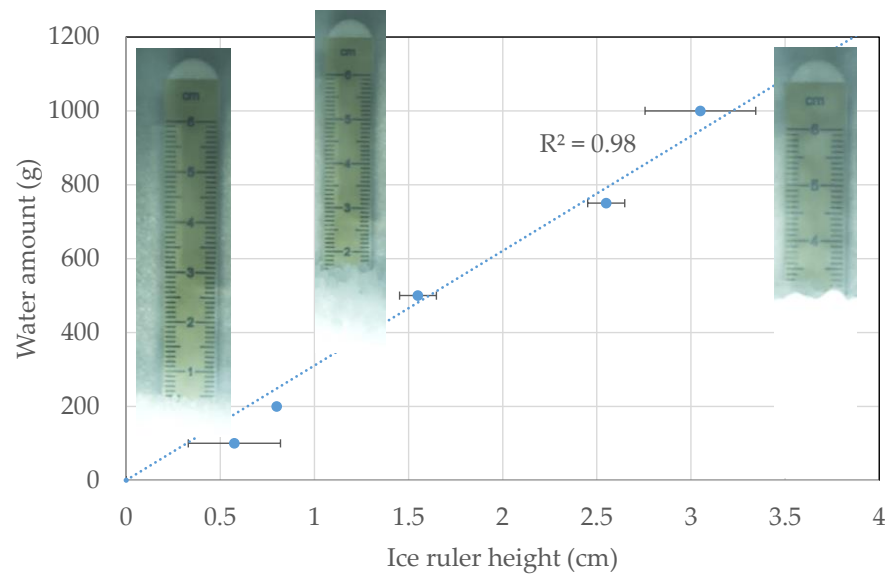


Figure A4. Ice ruler calibration.

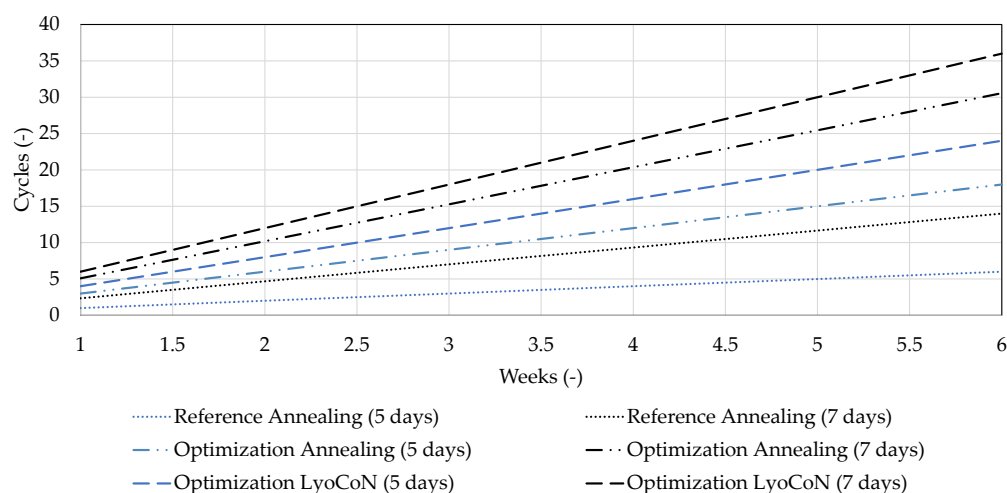


Figure A5. Productivity of different cycles for 5- and 7-day working week.

References

- Difranco, N. Lyophilization of Pharmaceuticals: An Overview. *Lubrizol CDMO [Online]*. 8 October 2019. Available online: <https://lubrizolcdmo.com/blog/lyophilization-of-pharmaceuticals-an-overview/> (accessed on 3 December 2020).
- Price, E. What is driving the growing demand for lyophilization? *PCI Synthesis [Online]*. 15 August 2019. Available online: <https://www.pcisynthesis.com/what-is-driving-the-growing-demand-for-lyophilization/> (accessed on 3 December 2020).
- Geidobler, R.; Winter, G. Controlled ice nucleation in the field of freeze-drying: Fundamentals and technology review. *Eur. J. Pharm. Biopharm.* **2013**, *85*, 214–222. [[CrossRef](#)]
- Rambhatla, S.; Ramot, R.; Bhugra, C.; Pikal, M.J. Heat and mass transfer scale-up issues during freeze drying: II. Control and characterization of the degree of supercooling. *AAPS PharmSciTech* **2004**, *5*, e58. [[CrossRef](#)] [[PubMed](#)]
- Konstantinidis, A.K.; Kuu, W.; Otten, L.; Nail, S.L.; Sever, R.R. Controlled nucleation in freeze-drying: Effects on pore size in the dried product layer, mass transfer resistance, and primary drying rate. *J. Pharm. Sci.* **2011**, *100*, 3453–3470. [[CrossRef](#)] [[PubMed](#)]
- Rambhatla, S.; Pikal, M.J. Heat and mass transfer scale-up issues during freeze-drying, I: Atypical radiation and the edge vial effect. *AAPS PharmSciTech* **2003**, *4*, E14. [[CrossRef](#)] [[PubMed](#)]
- Pikal, M.J.; Bogner, R.; Mudhivarathi, V.; Sharma, P.; Sane, P. Freeze-Drying Process Development and Scale-Up: Scale-Up of Edge Vial Versus Center Vial Heat Transfer Coefficients, Kv. *J. Pharm. Sci.* **2016**, *105*, 3333–3343. [[CrossRef](#)] [[PubMed](#)]
- Klepzig, L.S.; Juckers, A.; Knerr, P.; Harms, F.; Strube, J. Digital Twin for Lyophilization by Process Modeling in Manufacturing of Biologics. *Processes* **2020**, *8*, 1325. [[CrossRef](#)]
- Tang, X.; Pikal, M.J. Design of freeze-drying processes for pharmaceuticals: Practical advice. *Pharm. Res.* **2004**, *21*, 191–200. [[CrossRef](#)]
- Greiff, D. Development of cycles for lyophilization. *Dev. Biol. Stand.* **1992**, *74*, 85–92.
- EMA. ICH Guideline Q8 (R2) on Pharmaceutical Development. Available online: https://www.ema.europa.eu/en/documents/scientific-guideline/international-conference-harmonisation-technical-requirements-registration-pharmaceuticals-human-use_en-11.pdf (accessed on 24 June 2022).
- FDA. PAT—A Framework for Innovative Pharmaceutical Development, Manufacturing, and Quality Assurance. *FDA [Online]*, 11 June 2020. Available online: <https://www.fda.gov/regulatory-information/search-fda-guidance-documents/pat-framework-innovative-pharmaceutical-development-manufacturing-and-quality-assurance> (accessed on 15 February 2021).
- Thomas, F. Changing Perceptions: An Understanding of Lyophilization Advancements. *Pharm. Technol.* **2019**, *43*, 32–34.
- Kawasaki, H.; Shimanouchi, T.; Kimura, Y. Recent Development of Optimization of Lyophilization Process. *J. Chem.* **2019**, *2019*, 9502856. [[CrossRef](#)]
- Izutsu, K.; Yonemochi, E.; Yomota, C.; Goda, Y.; Okuda, H. Studying the morphology of lyophilized protein solids using X-ray micro-CT: Effect of post-freeze annealing and controlled nucleation. *AAPS PharmSciTech* **2014**, *15*, 1181–1188. [[CrossRef](#)] [[PubMed](#)]
- Gitter, J.H.; Geidobler, R.; Presser, I.; Winter, G. A Comparison of Controlled Ice Nucleation Techniques for Freeze-Drying of a Therapeutic Antibody. *J. Pharm. Sci.* **2018**, *107*, 2748–2754. [[CrossRef](#)]
- Vollrath, I.; Friess, W.; Freitag, A.; Hawe, A.; Winter, G. Comparison of ice fog methods and monitoring of controlled nucleation success after freeze-drying. *Int. J. Pharm.* **2019**, *558*, 18–28. [[CrossRef](#)] [[PubMed](#)]
- Juckers, A.; Knerr, P.; Harms, F.; Strube, J. Effect of the Freezing Step on Primary Drying Experiments and Simulation of Lyophilization Processes. *Processes* **2023**, *11*, 1404. [[CrossRef](#)]
- Juckers, A.; Knerr, P.; Harms, F.; Strube, J. Advanced Process Analytical Technology in Combination with Process Modeling for Endpoint and Model Parameter Determination in Lyophilization Process Design and Optimization. *Processes* **2021**, *9*, 1600. [[CrossRef](#)]

20. Juckers, A.; Knerr, P.; Harms, F.; Strube, J. Model-Based Product Temperature and Endpoint Determination in Primary Drying of Lyophilization Processes. *Pharmaceutics* **2022**, *14*, 809. [[CrossRef](#)] [[PubMed](#)]
21. Patel, S.M.; Doen, T.; Pikal, M.J. Determination of end point of primary drying in freeze-drying process control. *AAPS PharmSciTech* **2010**, *11*, 73–84. [[CrossRef](#)]
22. Schneid, S. Investigation of Novel Process Analytical Technology (PAT) Tools for Use in Freeze-Drying Processes. Ph.D. Thesis, Friedrich-Alexander-Universität Erlangen-Nürnberg (FAU), Erlangen, Germany, 2009.
23. Mayeresse, Y.; Veillon, R.; Sibille, P.H.; Nomine, C. Freeze-drying process monitoring using a cold plasma ionization device. *PDA J. Pharm. Sci. Technol.* **2007**, *61*, 160–174.
24. Barresi, A.A.; Pisano, R.; Fissore, D.; Rasetto, V.; Velardi, S.A.; Vallan, A.; Parvis, M.; Galan, M. Monitoring of the primary drying of a lyophilization process in vials. *Chem. Eng. Process. Process Intensif.* **2009**, *48*, 408–423. [[CrossRef](#)]
25. Assegehegn, G.; La Brito-de Fuente, E.; Franco, J.M.; Gallegos, C. Freeze-drying: A relevant unit operation in the manufacture of foods, nutritional products, and pharmaceuticals. *Adv. Food Nutr. Res.* **2020**, *93*, 1–58. [[CrossRef](#)]
26. De Beer, T.R.M.; Vercruyssen, P.; Burggraefe, A.; Quinten, T.; Ouyang, J.; Zhang, X.; Vervaet, C.; Remon, J.P.; Baeyens, W.R.G. In-line and real-time process monitoring of a freeze drying process using Raman and NIR spectroscopy as complementary process analytical technology (PAT) tools. *J. Pharm. Sci.* **2009**, *98*, 3430–3446. [[CrossRef](#)] [[PubMed](#)]
27. Brülls, M.; Folestad, S.; Sparén, A.; Rasmuson, A. In-situ near-infrared spectroscopy monitoring of the lyophilization process. *Pharm. Res.* **2003**, *20*, 494–499. [[CrossRef](#)] [[PubMed](#)]
28. Kauppinnen, A. *Raman and Near-Infrared Spectroscopic Methods for In-Line Monitoring of Freeze-Drying Process*; University of Eastern Finland: Kuopio, Finland, 2015; ISBN 78-952-61-1717-1.
29. Grohgan, H.; Gildemyn, D.; Skibsted, E.; Flink, J.M.; Rantanen, J. Rapid solid-state analysis of freeze-dried protein formulations using NIR and Raman spectroscopies. *J. Pharm. Sci.* **2011**, *100*, 2871–2875. [[CrossRef](#)] [[PubMed](#)]
30. Kauppinen, A.; Toiviainen, M.; Aaltonen, J.; Korhonen, O.; Järvinen, K.; Juuti, M.; Pellinen, R.; Ketolainen, J. Microscale freeze-drying with Raman spectroscopy as a tool for process development. *Anal. Chem.* **2013**, *85*, 2109–2116. [[CrossRef](#)] [[PubMed](#)]
31. Pieters, S.; Vander Heyden, Y.; Roger, J.-M.; D'Hondt, M.; Hansen, L.; Palagos, B.; de Spiegeleer, B.; Remon, J.-P.; Vervaet, C.; de Beer, T. Raman spectroscopy and multivariate analysis for the rapid discrimination between native-like and non-native states in freeze-dried protein formulations. *Eur. J. Pharm. Biopharm.* **2013**, *85*, 263–271. [[CrossRef](#)] [[PubMed](#)]
32. Preskar, M.; Korasa, K.; Vrbanec, T.; Klement, D.; Vrečer, F.; Gašperlin, M. Applicability of Raman and near-infrared spectroscopy in the monitoring of freeze-drying injectable ibuprofen. *Drug Dev. Ind. Pharm.* **2021**, *47*, 758–769. [[CrossRef](#)] [[PubMed](#)]
33. Romero-Torres, S.; Wikström, H.; Grant, E.R.; Taylor, L.S. Monitoring of mannitol phase behavior during freeze-drying using non-invasive Raman spectroscopy. *PDA J. Pharm. Sci. Technol.* **2007**, *61*, 131–145. [[PubMed](#)]
34. Sampathkumar, K.; Cao, W.; Phillips, J.; Amgen, P. Applying Raman Spectroscopy to Design of Lyophilization Cycles for Protein Formulation Development. *Am. Pharm. Rev.* **2009**, *12*, 44–48.
35. Sarraguça, M.C.; de Beer, T.; Vervaet, C.; Remon, J.-P.; Lopes, J.A. A batch modelling approach to monitor a freeze-drying process using in-line Raman spectroscopy. *Talanta* **2010**, *83*, 130–138. [[CrossRef](#)]
36. Su, W.; Hao, H.; Glennon, B.; Barrett, M. Spontaneous Polymorphic Nucleation of d -Mannitol in Aqueous Solution Monitored with Raman Spectroscopy and FBRM. *Cryst. Growth Des.* **2013**, *13*, 5179–5187. [[CrossRef](#)]
37. De Beer, T.; Burggraefe, A.; Fonteyne, M.; Saerens, L.; Remon, J.P.; Vervaet, C. Near infrared and Raman spectroscopy for the in-process monitoring of pharmaceutical production processes. *Int. J. Pharm.* **2011**, *417*, 32–47. [[CrossRef](#)] [[PubMed](#)]
38. Moino, C.; Bourlés, E.; Pisano, R.; Scutellà, B. In-Line Monitoring of the Freeze-Drying Process by Means of Heat Flux Sensors. *Ind. Eng. Chem. Res.* **2021**, *60*, 9637–9645. [[CrossRef](#)]
39. Chen, R.; Slater, N.K.H.; Gatlin, L.A.; Kramer, T.; Shalae, E.Y. Comparative rates of freeze-drying for lactose and sucrose solutions as measured by photographic recording, product temperature, and heat flux transducer. *Pharm. Dev. Technol.* **2008**, *13*, 367–374. [[CrossRef](#)] [[PubMed](#)]
40. Carfagna, M.; Rosa, M.; Hawe, A.; Frieß, W. Design of freeze-drying cycles: The determination of heat transfer coefficient by using heat flux sensor and MicroFD. *Int. J. Pharm.* **2022**, *621*, 121763. [[CrossRef](#)] [[PubMed](#)]
41. Vollrath, I. *Controlled Nucleation and Heat Flux Measurements as Innovative Technologies for Freeze-Drying*; Ludwig-Maximilians-Universität München: München, Germany, 2018.
42. Vollrath, I.; Pauli, V.; Friess, W.; Freitag, A.; Hawe, A.; Winter, G. Evaluation of Heat Flux Measurement as a New Process Analytical Technology Monitoring Tool in Freeze Drying. *J. Pharm. Sci.* **2017**, *106*, 1249–1257. [[CrossRef](#)] [[PubMed](#)]
43. Carfagna, M.; Rosa, M.; Lucke, M.; Hawe, A.; Frieß, W. Heat flux sensor to create a design space for freeze-drying development. *Eur. J. Pharm. Biopharm.* **2020**, *153*, 84–94. [[CrossRef](#)] [[PubMed](#)]
44. Presser, I. *Innovative Online Messverfahren zur Optimierung von Gefriertrocknungsprozessen*; Ludwig-Maximilians-Universität München: München, Germany, 2003.
45. Patel, S.M.; Pikal, M. Process analytical technologies (PAT) in freeze-drying of parenteral products. *Pharm. Dev. Technol.* **2009**, *14*, 567–587. [[CrossRef](#)]
46. Ganguly, A.; Stewart, J.; Rhoden, A.; Volny, M.; Saad, N. Mass spectrometry in freeze-drying: Motivations for using a bespoke PAT for laboratory and production environment. *Eur. J. Pharm. Biopharm.* **2018**, *127*, 298–308. [[CrossRef](#)]
47. Tang, X.C.; Nail, S.L.; Pikal, M.J. Evaluation of manometric temperature measurement (MTM), a process analytical technology tool in freeze drying, part III: Heat and mass transfer measurement. *AAPS PharmSciTech* **2006**, *7*, 97. [[CrossRef](#)]

48. Fissore, D.; Pisano, R.; Barresi, A.A. On the Methods Based on the Pressure Rise Test for Monitoring a Freeze-Drying Process. *Dry. Technol.* **2010**, *29*, 73–90. [[CrossRef](#)]
49. Lewis, L.M.; Johnson, R.E.; Oldroyd, M.E.; Ahmed, S.S.; Joseph, L.; Saracovan, I.; Sinha, S. Characterizing the freeze-drying behavior of model protein formulations. *AAPS PharmSciTech* **2010**, *11*, 1580–1590. [[CrossRef](#)] [[PubMed](#)]
50. Milton, N.; Pikal, M.J.; Roy, M.L.; Nail, S.L. Evaluation of manometric temperature measurement as a method of monitoring product temperature during lyophilization. *PDA J. Pharm. Sci. Technol.* **1997**, *51*, 7–16. [[PubMed](#)]
51. Tang, X.C.; Nail, S.L.; Pikal, M.J. Freeze-drying process design by manometric temperature measurement: Design of a smart freeze-dryer. *Pharm. Res.* **2005**, *22*, 685–700. [[CrossRef](#)] [[PubMed](#)]
52. Tang, X.C.; Nail, S.L.; Pikal, M.J. Evaluation of manometric temperature measurement, a process analytical technology tool for freeze-drying: Part II measurement of dry-layer resistance. *AAPS PharmSciTech* **2006**, *7*, 93. [[CrossRef](#)] [[PubMed](#)]
53. Awotwe Otoo, D.; Agarabi, C.; Khan, M.A. An integrated process analytical technology (PAT) approach to monitoring the effect of supercooling on lyophilization product and process parameters of model monoclonal antibody formulations. *J. Pharm. Sci.* **2014**, *103*, 2042–2052. [[CrossRef](#)] [[PubMed](#)]
54. Gieseler, H.; Kessler, W.J.; Finson, M.; Davis, S.J.; Mulhall, P.A.; Bons, V.; Debo, D.J.; Pikal, M.J. Evaluation of tunable diode laser absorption spectroscopy for in-process water vapor mass flux measurements during freeze drying. *J. Pharm. Sci.* **2007**, *96*, 1776–1793. [[CrossRef](#)] [[PubMed](#)]
55. Kuu, W.Y.; Nail, S.L. Rapid freeze-drying cycle optimization using computer programs developed based on heat and mass transfer models and facilitated by tunable diode laser absorption spectroscopy (TDLAS). *J. Pharm. Sci.* **2009**, *98*, 3469–3482. [[CrossRef](#)]
56. Kuu, W.Y.; O'Bryan, K.R.; Hardwick, L.M.; Paul, T.W. Product mass transfer resistance directly determined during freeze-drying cycle runs using tunable diode laser absorption spectroscopy (TDLAS) and pore diffusion model. *Pharm. Dev. Technol.* **2011**, *16*, 343–357. [[CrossRef](#)]
57. Jameel, F.; Kessler, W.J.; Schneid, S. Application of PAT in Real-time Monitoring and Controlling of Lyophilization Process. In *Quality by Design for Biopharmaceutical Drug Product Development*; Jameel, F., Hershenson, S., Khan, M.A., Martin-Moe, S., Eds.; Springer: New York, NY, USA, 2015; pp. 605–647. ISBN 978-1-4939-2315-1.
58. Kessler, W.J.; Gong, E. Tunable Diode Laser Absorption Spectroscopy in Lyophilization. In *Lyophilization of Pharmaceuticals and Biologicals*; Ward, K.R., Matejtschuk, P., Eds.; Springer: New York, NY, USA, 2019; pp. 113–141. ISBN 978-1-4939-8927-0.
59. Sharma, P.; Kessler, W.J.; Bogner, R.; Thakur, M.; Pikal, M.J. Applications of the Tunable Diode Laser Absorption Spectroscopy: In-Process Estimation of Primary Drying Heterogeneity and Product Temperature During Lyophilization. *J. Pharm. Sci.* **2019**, *108*, 416–430. [[CrossRef](#)]
60. Aydin, E.S.; Yucel, O.; Sadikoglu, H. Modelling and simulation of a moving interface problem: Freeze drying of black tea extract. *Heat Mass Transf.* **2017**, *53*, 2143–2154. [[CrossRef](#)]
61. Bano, G.; De-Luca, R.; Tomba, E.; Marcelli, A.; Bezzo, F.; Barolo, M. Primary Drying Optimization in Pharmaceutical Freeze-Drying: A Multivial Stochastic Modeling Framework. *Ind. Eng. Chem. Res.* **2020**, *59*, 5056–5071. [[CrossRef](#)]
62. Song, C.S.; Nam, J.H. A Numerical Study on Freeze Drying Characteristics of Cylindrical Products with and without Container. *Int. J. Transp. Phenom.* **2005**, *7*, 241–254.
63. Mascarenhas, W.J.; Akay, H.U.; Pikal, M.J. A computational model for finite element analysis of the freeze-drying process. *Comput. Methods Appl. Mech. Eng.* **1997**, *148*, 105–124. [[CrossRef](#)]
64. Pikal, M.J.; Mascarenhas, W.J.; Akay, H.U.; Cardon, S.; Bhugra, C.; Jameel, F.; Rambhatla, S. The Nonsteady State Modeling of Freeze Drying: In-Process Product Temperature and Moisture Content Mapping and Pharmaceutical Product Quality Applications. *Pharm. Dev. Technol.* **2005**, *10*, 17–32. [[CrossRef](#)] [[PubMed](#)]
65. Ravnik, J.; Golobič, I.; Sitar, A.; Avanzo, M.; Irman, Š.; Kočevar, K.; Cegnar, M.; Zadavec, M.; Ramšak, M.; Hriberšek, M. Lyophilization model of mannitol water solution in a laboratory scale lyophilizer. *J. Drug Deliv. Sci. Technol.* **2018**, *45*, 28–38. [[CrossRef](#)]
66. Sheehan, P.; Liapis, A.I. Modeling of the primary and secondary drying stages of the freeze drying of pharmaceutical products in vials: Numerical results obtained from the solution of a dynamic and spatially multi-dimensional lyophilization model for different operational policies. *Biotechnol. Bioeng.* **1998**, *60*, 712–728. [[CrossRef](#)]
67. Song, C.S.; Nam, J.H.; Kim, C.-J.; Ro, S.T. Temperature distribution in a vial during freeze-drying of skim milk. *J. Food Eng.* **2005**, *67*, 467–475. [[CrossRef](#)]
68. Srinivasan, G.; Muneeshwaran, M.; Raja, B. Numerical investigation of heat and mass transfer behavior of freeze drying of milk in vial. *Heat Mass Transf.* **2019**, *55*, 2073–2081. [[CrossRef](#)]
69. Vilas, C.; Alonso, A.; Balsa-Canto, E.; López-Quiroga, E.; Trelea, I.C. Model-Based Real Time Operation of the Freeze-Drying Process. *Processes* **2020**, *8*, 325. [[CrossRef](#)]
70. Velardi, S.A.; Barresi, A.A. Development of simplified models for the freeze-drying process and investigation of the optimal operating conditions. *Chem. Eng. Res. Des.* **2008**, *86*, 9–22. [[CrossRef](#)]
71. Fissore, D.; Pisano, R.; Barresi, A.A. Applying quality-by-design to develop a coffee freeze-drying process. *J. Food Eng.* **2014**, *123*, 179–187. [[CrossRef](#)]

72. Leys, L.; Vanbillemont, B.; van Bockstal, P.J.; Lammens, J.; Nuytten, G.; Corver, J.; Vervaet, C.; de Beer, T. A primary drying model-based comparison of conventional batch freeze-drying to continuous spin-freeze-drying for unit doses. *Eur. J. Pharm. Biopharm.* **2020**, *157*, 97–107. [[CrossRef](#)] [[PubMed](#)]
73. Fissore, D.; Barresi, A.A. Scale-up and Process Transfer of Freeze-Drying Recipes. *Dry. Technol.* **2011**, *29*, 1673–1684. [[CrossRef](#)]
74. Fissore, D.; Pisano, R. Computer-Aided Framework for the Design of Freeze-Drying Cycles: Optimization of the Operating Conditions of the Primary Drying Stage. *Processes* **2015**, *3*, 406–421. [[CrossRef](#)]
75. Fissore, D.; Pisano, R.; Barresi, A.A. Advanced approach to build the design space for the primary drying of a pharmaceutical freeze-drying process. *J. Pharm. Sci.* **2011**, *100*, 4922–4933. [[CrossRef](#)] [[PubMed](#)]
76. Giordano, A.; Barresi, A.A.; Fissore, D. On the use of mathematical models to build the design space for the primary drying phase of a pharmaceutical lyophilization process. *J. Pharm. Sci.* **2011**, *100*, 311–324. [[CrossRef](#)]
77. Koganti, V.R.; Shalaev, E.Y.; Berry, M.R.; Osterberg, T.; Youssef, M.; Hiebert, D.N.; Kanka, F.A.; Nolan, M.; Barrett, R.; Scalzo, G.; et al. Investigation of design space for freeze-drying: Use of modeling for primary drying segment of a freeze-drying cycle. *AAPS PharmSciTech* **2011**, *12*, 854–861. [[CrossRef](#)]
78. Vanbillemont, B.; Nicolai, N.; Leys, L.; de Beer, T. Model-Based Optimisation and Control Strategy for the Primary Drying Phase of a Lyophilisation Process. *Pharmaceutics* **2020**, *12*, 181. [[CrossRef](#)]
79. Mortier, S.T.F.C.; van Bockstal, P.-J.; Corver, J.; Nopens, I.; Gernaey, K.V.; de Beer, T. Uncertainty analysis as essential step in the establishment of the dynamic Design Space of primary drying during freeze-drying. *Eur. J. Pharm. Biopharm.* **2016**, *103*, 71–83. [[CrossRef](#)]
80. Rajniak, P.; Moreira, J.; Tsinontides, S.; Pham, D.; Bermingham, S. Integrated use of mechanistic models and targeted experiments for development, scale-up and optimization of lyophilization cycles: A single vial approach for primary drying. *Dry. Technol.* **2022**, *40*, 310–325. [[CrossRef](#)]
81. Zhou, D.; Shang, S.; Tharp, T.; Jameel, F.; Sinha, K.; Nere, N.K. Leveraging Lyophilization Modeling for Reliable Development, Scale-up and Technology Transfer. *AAPS PharmSciTech* **2019**, *20*, 263. [[CrossRef](#)] [[PubMed](#)]
82. Zhu, T.; Moussa, E.M.; Witting, M.; Zhou, D.; Sinha, K.; Hirth, M.; Gastens, M.; Shang, S.; Nere, N.; Somashekar, S.C.; et al. Predictive models of lyophilization process for development, scale-up/tech transfer and manufacturing. *Eur. J. Pharm. Biopharm.* **2018**, *128*, 363–378. [[CrossRef](#)] [[PubMed](#)]
83. Tchessalov, S.; Latshaw, D.; Nulu, S.; Bentley, M.; Tharp, T.; Ewan, S.; Chen, X. Application of First Principles Primary Drying Model to Lyophilization Process Design and Transfer: Case Studies from the Industry. *J. Pharm. Sci.* **2021**, *110*, 968–981. [[CrossRef](#)] [[PubMed](#)]
84. Vanbillemont, B.; Greiner, A.-L.; Ehrl, V.; Menzen, T.; Friess, W.; Hawe, A. A model-based optimization strategy to achieve fast and robust freeze-drying cycles. *Int. J. Pharm. X* **2023**, *5*, 100180. [[CrossRef](#)]
85. Udugama, I.A.; Lopez, P.C.; Gargalo, C.L.; Li, X.; Bayer, C.; Gernaey, K.V. Digital Twin in biomanufacturing: Challenges and opportunities towards its implementation. *Syst. Microbiol. Biomanuf.* **2021**, *1*, 257–274. [[CrossRef](#)]
86. Schmidt, A.; Helgers, H.; Vetter, F.L.; Juckers, A.; Strube, J. Digital Twin of mRNA-Based SARS-COVID-19 Vaccine Manufacturing towards Autonomous Operation for Improvements in Speed, Scale, Robustness, Flexibility and Real-Time Release Testing. *Processes* **2021**, *9*, 748. [[CrossRef](#)]
87. Helgers, H.; Hengelbrock, A.; Schmidt, A.; Vetter, F.L.; Juckers, A.; Strube, J. Digital Twins for scFv Production in Escherichia coli. *Processes* **2022**, *10*, 809. [[CrossRef](#)]
88. Hengelbrock, A.; Helgers, H.; Schmidt, A.; Vetter, F.L.; Juckers, A.; Rosengarten, J.F.; Stitz, J.; Strube, J. Digital Twin for HIV-Gag VLP Production in HEK293 Cells. *Processes* **2022**, *10*, 866. [[CrossRef](#)]
89. Juckers, A.; Knerr, P.; Harms, F.; Strube, J. Emerging PAT for Freeze-Drying Processes for Advanced Process Control. *Processes* **2022**, *10*, 2059. [[CrossRef](#)]
90. Wegiel, L.A.; Ferris, S.J.; Nail, S.L. Experimental Aspects of Measuring the Vial Heat Transfer Coefficient in Pharmaceutical Freeze-Drying. *AAPS PharmSciTech* **2018**, *19*, 1810–1817. [[CrossRef](#)]
91. Rambhatla, S.; Tchessalov, S.; Pikal, M.J. Heat and mass transfer scale-up issues during freeze-drying. III: Control and characterization of dryer differences via operational qualification tests. *AAPS PharmSciTech* **2006**, *7*, E39. [[CrossRef](#)] [[PubMed](#)]
92. Liapis, A.I.; Sadikoglu, H. Dynamic pressure rise in the drying chamber as a remote sensing method for monitoring the temperature of the product during the primary drying stage of freeze drying. *Dry. Technol.* **1998**, *16*, 1153–1171. [[CrossRef](#)]
93. Andrieu, J.; Vessot, S. A review on experimental determination and optimization of physical quality factors during pharmaceuticals freeze-drying cycles. *Dry. Technol.* **2018**, *36*, 129–145. [[CrossRef](#)]
94. Stratta, L.; Capozzi, L.C.; Franzino, S.; Pisano, R. Economic Analysis of a Freeze-Drying Cycle. *Processes* **2020**, *8*, 1399. [[CrossRef](#)]

Disclaimer/Publisher’s Note: The statements, opinions and data contained in all publications are solely those of the individual author(s) and contributor(s) and not of MDPI and/or the editor(s). MDPI and/or the editor(s) disclaim responsibility for any injury to people or property resulting from any ideas, methods, instructions or products referred to in the content.